Modelling and Simulation of Filopodial Protrusion

by

Tochukwu Chinedu Ezeanochie

Thesis submitted to the

Faculty of Graduate and Postdoctoral Studies

In partial fulfillment of the requirements

For the M.A.Sc. degree in

Mechanical Engineering

Ottawa-Carleton Institute for Mechanical and Aerospace Engineering
Faculty of Engineering
University of Ottawa

Abstract

The effect of substrate surface topology on the interaction of living cells with inanimate substrates is a well-established phenomenon. When cells are placed on biomaterials, they outgrow protrusions called filopodia that sense surface features in their immediate surroundings and initiate the formation of stable cell adhesion complexes closer to the cell body. Adhesion proteins permit filopodia to constantly explore the surrounding microenvironment. A better understanding of the relationship of filopodia with surface features is highly relevant for exploiting custom-made surfaces to guide cell activity.

In this work, mathematical modeling and simulation were used to describe different phenomena related to the interaction of a filopodium with its microenvironment, with the aim of reproducing experimentally observed phenomena associated to filopodia growth and interactions with substrates. The Kelvin Voigt model was used for the viscoelastic response of filopodia. Result predict filopodia protrusion under test conditions and helps improving our understanding on the effect of substrate topology on the biomechanical response of filopodial extensions.

Keywords: Filopodia; Adhesion; Beam; Model; Substrate.

Acknowledgements

I would like to thank my supervisors Davide Spinello and Fabio Variola for their guidance, mentorship, patience and high expectations throughout the completion of this study. Also, I would like to thank University of Ottawa, Faculty of Engineering and the Department of Mechanical Engineering for their support and my friends who have encouraged me with their uplifted spirits. Last, and by far not the least, I'd thank my parents, who have always given me their support in all things; without them, none of my work could never have come to pass.

Table of Contents

List of Tables

List of Figures

Nomenclature

S_0	Uniform attraction exerted on the filopodia.
E	Young modulus of a filopodium
I	Area moment of inertia
p	Transverse distributed force
Δh	Deflection at the tip of each filopodium
F_{buckle}	Critical force that buckle the rods
K_BT	Thermal energy
L_P	F-actin persistence length
$I(N)$	Non-dimensional factor
L_{max}^{b}	Critical length at which the membrane resistances force buckles the filopodia
W	Deflection of the beam
M	Moment resultant
u	Elongation of the beam
A	Cross section area (πr^2)
k	Stiffness
D	Diameter of a filopodium
δ	Gap between the filopodium and the substrate
W	Weight of a filopodium
L	Length of a filopodium
EI	Bending stiffness of a filopodium
EA	Axial stiffness of a filopodium
f	Force at the tip of the filopodium
k_{filo}	Elastic Modulus of the experimental model
C_{filo}	Viscosity
v_{poly}	Polymerization at the tip

b_{int}	Actin membrane linkage at the tip
k_{eff}	Elastic force stiffness controlled by the optical trap
θ	Rotation of a cross section
κ	Curvature of the deflected longitudinal axis
P	Population
c	Growth rate

Acronyms

ECM	Extracellular matrix
ATP	Adenosine Triphosphate
F-actin	Filamentous actin
SEM	Scanning electron microscope
TEM	Transmission electron microscope
AFM	Atomic force Microscope
QPD	Quadrant Photo diode

Chapter 1

Introduction

1.1 Motivation

Many systems in biomedical engineering involve the study of living cells and their interaction with prosthetic materials [1]. This study is of great interest to the field of biomedical engineering. It helps in the development of innovative strategies in tissue engineering and leads to the advancement of prosthetic devices [2, 3]. Living cells require molecular recognition and guiding interaction cues to regulate their pathway to prosthetic materials [4]. Due to its mechanical properties, filopodia found in living cells are able to crawl to strategic sites and sense the surface features of their immediate environment. Figure 1.1 shows a cell-substrate interaction. However this mechanism of the filopodia formation has not been completely understood. There are two theories, nowadays that model the formation of filopodia: the convergent elongation and tip nucleation [5] . An example of these entities are shown in Figure 1.2. In the framework of these latest development, in this thesis, we developed a simple mechanical model that allows to predict the behavior of these complex systems. This was done, in order to be able to explain mechanisms related to growth and interaction with the environment based on simple physics and mechanics. A distributed mechanical model consisting of a Kelvin Voigt model is considered for the filopodium. This models can be tuned so that it can reproduce experimental results in which the viscoelastic response of a filopodial protrusion can be measured under different conditions.

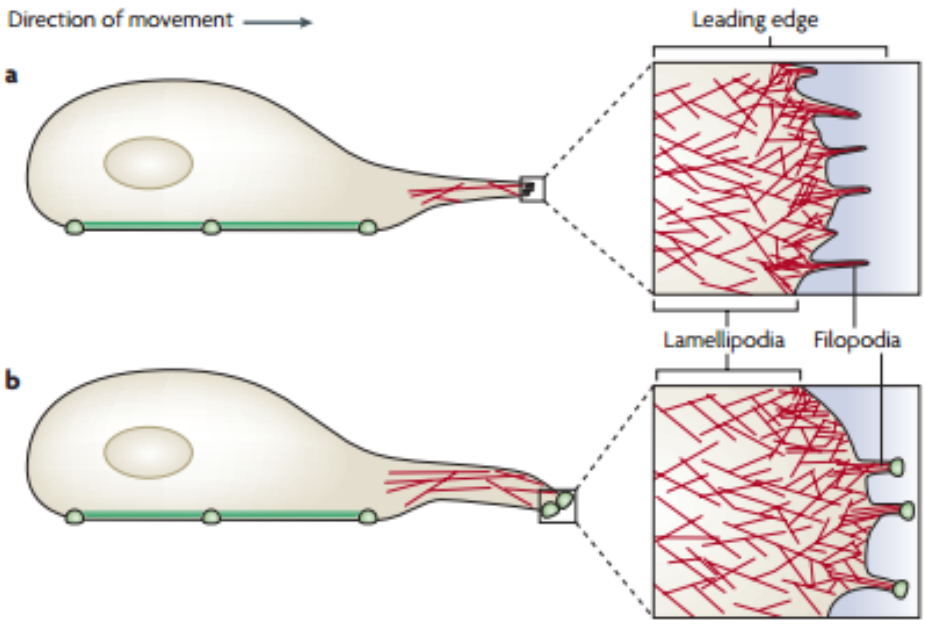

Figure 1.1: Cell migration is dependent on the filopodia [6].

1.2 Microscopic overview

At the microscopic level, the activity between the cell and the substrate is determined by the adhesion between them. Modeling and experimental studies have attempted to explain the mechanism that regulates this adhesion [7]. Recent work explains the physics behind this adhesion mechanism by relating the active reproduction of mechanical forces on the interface of the cell-substrate [2]. These forces caused by the adhesion are conveyed to the substrate through focal adhesions, which are large, dynamic adhesion force clusters in a cell [8]. These focal adhesions are used by cells to sense the physical properties of the substrate. The effect of these forces is intricately linked to the material properties of cells and the substrate.

1.3 Cellular overview

At the cellular level, cells adheres to substrates by migrating to strategic sites for interaction to take place between it and the substrates. Thin, finger-like protrusions known as filopodia found at the leading edge of these migrating cells are cellular organelles with primary sensory functions [6]. These protrusions are composed of various organic substances such as proteins, working together through an intermingled web of chemical reactions, mechanical interactions and diffusions. These chemical reactions have controlling functions such as promoting reactions whereby actin molecules, a globular multi-functional protein, interact chemically to form a single chain [9]. This process is known as actin polymerization, and the single chain is called an actin filament.

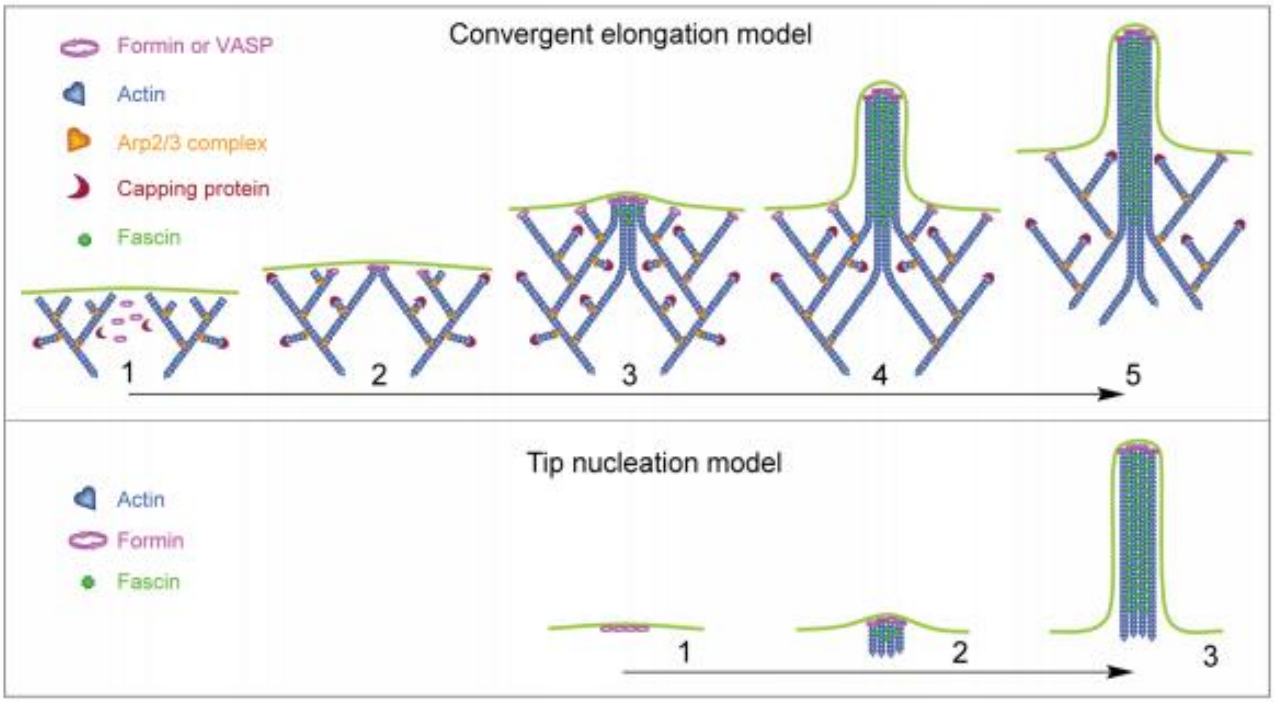

Figure 1.2 Mechanistic models of filopodia initiation. Convergent elongation model (top) Tip nucleation model (bottom) [5]

The molecules that mediate the attachment between a cell and its surroundings (transmembrane molecules) can be present in an unclustered but activated state at the tip or along the shaft of the filopodia. They can also be present in more organized adhesion clusters (i.e. focal complexes) which can be situated at the tip, along the shaft and at the base.

From a lamellipodium which is a three dimensional mesh of actin filaments, a filopodium extends to probe the microenvironment for mechanical obstacles and cues. A filopodium can grow, pause, retract and change speed in between dynamical regimes [9]. This is due to the internal regulation and response to changes in the microenvironment [10]. Examples of cells that make use of a filopodium are fibroblasts, neurons growth axons during embryonic development, wound healing cells and metastatic cancer cells [11]. As well as the sensory functions, filopodia have recently been proven to partake in vital mechanical roles involving epithelial adhesion (cell-cell adhesion) [9].

1.4 Subject and scope of this work

This study explored the mechanism of filopodia protrusion on substrates. The goal is to develop a simple mechanical model to predict the behavior of these complex systems, and to explain mechanisms related to growth and interaction with the environment based on simple physics and mechanics. This work is structured into three interconnected sections, which provide a better understanding of the nature of a filopodium. These section are:

1. The first section discusses the mathematical model of a filopodium protrusion.
2. The second section discusses the estimation of constitutive parameters of a filopodium from a body of literature that is mainly focused on an experiment.
3. The third section discusses the natural behaviour and characteristics of an extending

filopodium crossing over an asperity in the substrate.

1.5 Objective and significance of the work

Filopodia in living cells were first investigated in 1961 [11]. Its substrate-exploring functions were suggested in 1976, and assumed to be regulated by mechanical forces [7]. Numerous studies have focused on understanding mechanisms behind these entities, this could lead to a better understanding of filopodia behavior [12, 13]. Models have been developed with the intention of mimicking the filopodia [14, 15]. However, these models were only able to study the filopodia formation and did not consider the effect of the filopodia protrusion on a substrate. A better understanding of the relationship of filopodia with surface features is highly relevant for exploiting custom-made surfaces to guide cell activity. The model developed in this thesis is important for the following reasons:

- This model can help to identify experimental parameters for specifying and estimating filopodial activity, which increase the efficiency of experimental efforts.
- The model predicts filopodial protrusion under a set of given conditions, which can be used to strengthen experimental database and study patterns of filopodia behavior. Figure 1.2 shows the view of a filopodia and its mesh network.

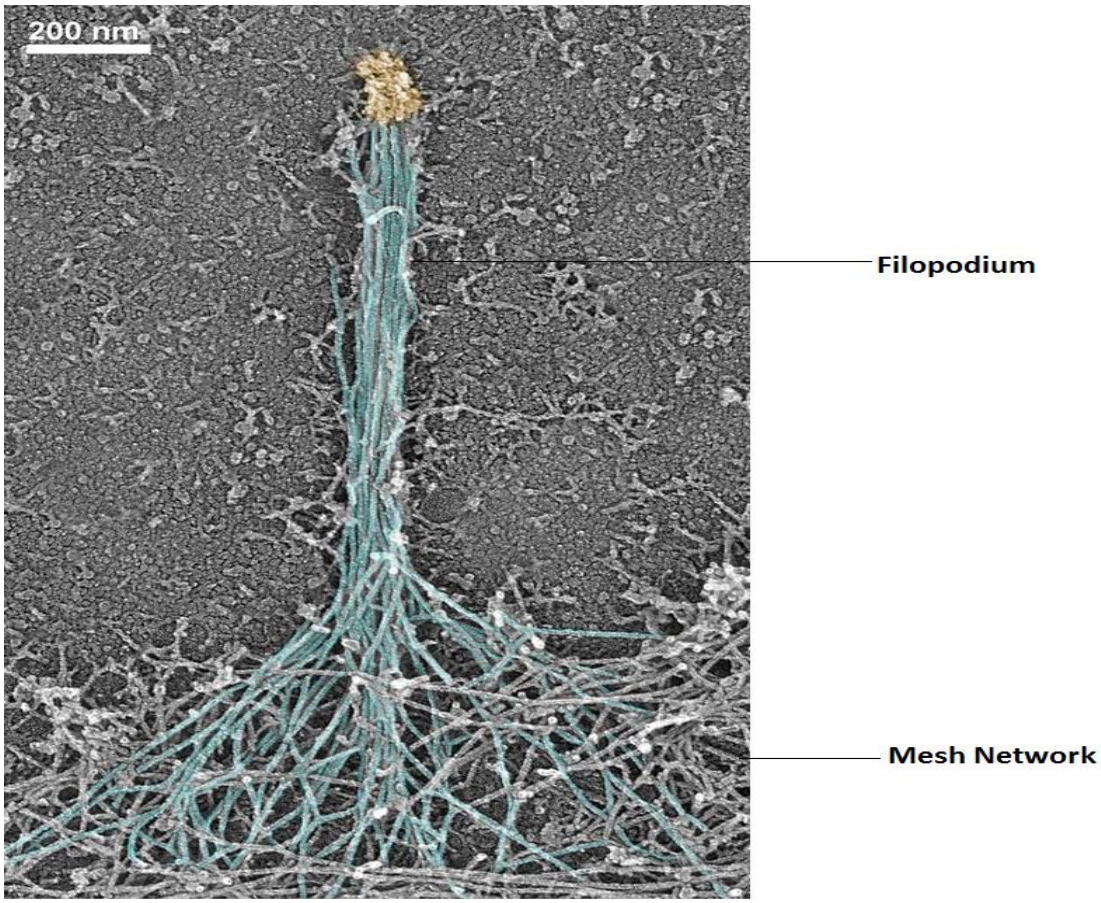

Figure 1.3: View of a filopodium and its mesh network [16]

1.6 Thesis organization

The following five chapters map out the steps taken to study the interaction between these living cells and prosthetic materials. Chapter 2 discusses the literature review on the filopodial adhesion to a substrate. Chapter 3 explains the model used for the filopodia and the estimation of the constitutive parameters. Chapter 4 examines the results obtained from simulations and its validation. Finally, Chapter 5 summarizes and concludes the work been done.

Chapter 2

Literature review

2.1 Filopodia Functions

William Wood et al [11] studied the structure of a filopodium. The study explains the mechanical role of filopodia, which includes the investigation of the extracellular matrix (ECM) and surfaces of other cells. It also includes recognizing suitable targets for adhesion or in the case of a migrating growth cone[1], for sensing guidance cues that enable the axon[2] to navigate to its proper target. In addition to this sensory role, filopodia have also recently been shown to play an important role in epithelial adhesion as shown in figure 2.1, and are also likely to be key players in evolving processes that need migrating epithelial sheets[3] to zipper and fuse to one another.

[1] A growth cone is a dynamic, actin -supported extension of a developing neurite seeking its synaptic target

[2] also known as a nerve fibre, is a long, slender projection of a nerve cell, or neuron, that typically conducts electrical impulses away from the neuron's cell body

[3] Epithelium is one of the four basic types of animal tissue, along with connective tissue, muscle tissue and nervous tissue. Epithelial tissues line the cavities and surfaces of structures throughout the body

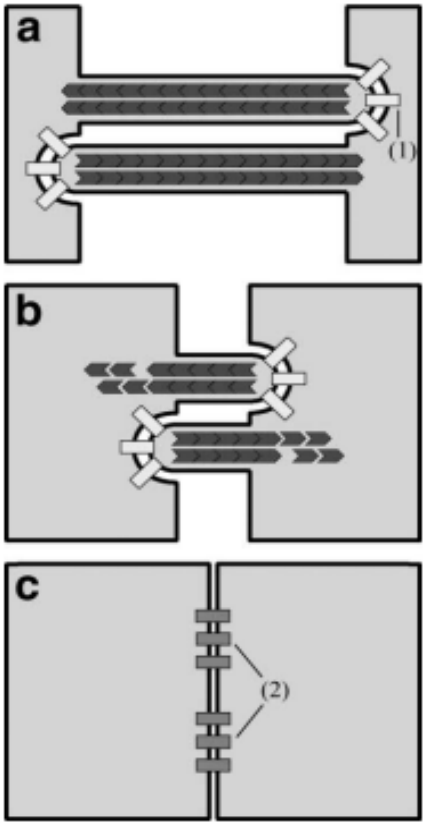

Figure 2.1 Filopodial function during epithelial adhesion (a) Filopodia from two opposing cells interdigitate across the mid-line, forming weak adhesions at sites of membrane contact (b) Filopodia then regress through actin de-polymerization and subsequently(c) weak adhesions evolve into mature adherents junctions [11].

Another study by Roger W Davenport [17], explained the sensory role for neuronal growth cone filopodia. The study suggest that because of dynamic nature of the neuronal growth cone filopodia, the filopodia can sample their immediate environment and respond to environment signals that affect the growth cone behavior and shape. Filopodia are also well positioned to serve as antenna-like sensors, their extensive span allows sampling of information over a greatly enhanced radius. The study further showed that the neuronal growth cone filopodia contain signal transduction mechanism that allow independent responses and the spread of distant environment information to their parent growth cone. In conclusion, because the

filopodia are small, motile and transient structure, it may need less energy to extend than the much large mass of the growth cone. They can act as competent sensory probes. Their large surface area to volume ratio equated with the growth cone makes them highly sensitive to environmental signals. They are isolated individuals extending in a fan-like fashion across the front of the growth cone, they enable growth cones to sense information from different zone concurrently and separately. Hence filopodia are a fundamental unit of organization for neuronal path finding.

Albuschies et al [7] observed the role of the filopodia in the recognition of nanotopographies. Highly flexible hairy silicon nanowires were used to model a filopodium on micropatterned surface. Confocal microscopy and electron microscopy were used to image the initial filopodia contact and observe how the cellular processes of adhesion, spreading, migration and division in the absence of the Lamellipodia are affected by this interaction. The authors ultimately deduced that a filopodium tilts and lines with a substrate when it comes in contact with it. The dynamics of the angle of contact between the filopodia and the substrate was also an important factor in determining if the filopodia adhesion would break or mature. This study highlights the vital role the filopodia plays in directing topographical preferences.

Similarly, Mogilner et al [10] explained the physics of filopodia protrusion. In their study, they used a numerical model to determine the mechanics and spacing dynamics of the actin filament in a filopodium. The model demonstrated that 10-30 actin filaments needed to be bundled at 12nm apart to overcome the membrane resistance, which is the measure of weakness of the trans-membrane flow of protein. This model suggests that 10-30 filaments are present in the filopodia length to prevent buckling. The model also deduced that 30 filaments are present in a filopodium length that prevents contraction by the G-actin and myosin protein

that accumulates at the tip of the cell. The myosin is a family of the ATP-dependent motor proteins known for their role in muscle contraction and cell motility. The authors also demonstrated that a filopodium is made up of a filamentous actin (F-actin) filament and that F-actin barbed ends needed to be fixated and sealed, to house the required number of filopodia. From [10], 10-30 actin filaments are needed for the filopodia model. Figure 2.2 illustrates the organization and characteristics scale of a filopodia and lamellipodia. Furthermore, according to Mellor [18], the filopodia have circular cross sections. This knowledge is used to compute the area and area moment of inertia of filopodia in this thesis.

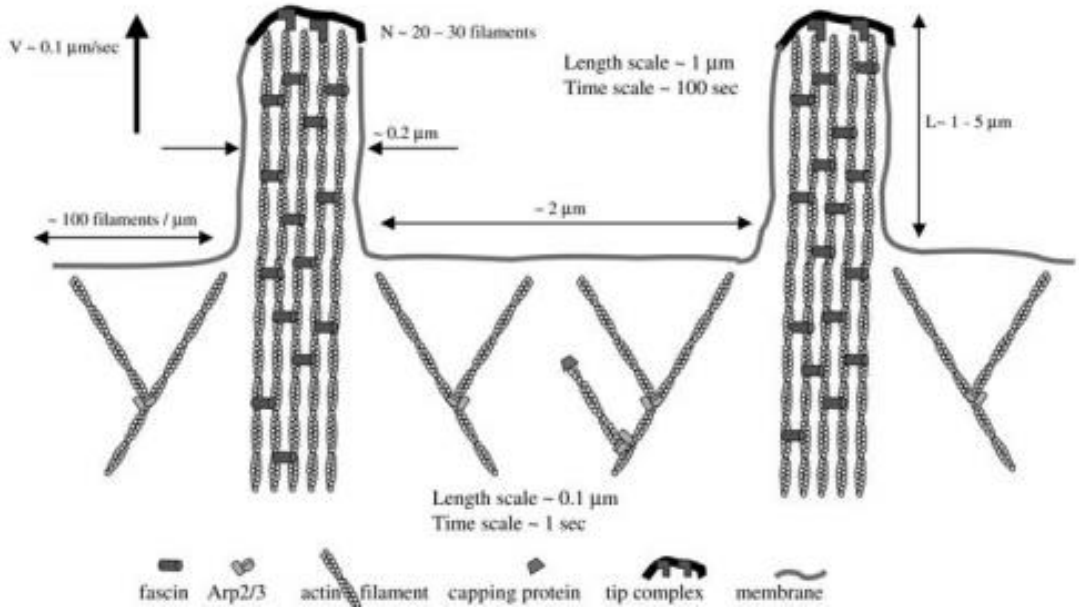

Figure 2.2: Organization and characteristics scale of a filopodia and Lamellipodia [10].

2.2 The role of filopodia in the interaction between cells and substrates

Previous studies have investigated the interaction of filopodia with their microenvironments. Harrison [19] first discovered the vital role of substrate topography for adhesions of filopodia, by exploring its influence on the protruding nerve fiber. The nerve fiber is a thread-like extension of a nerve cell which conducts impulses from the boundary of the body to the central nervous system as shown in figure 2.3.

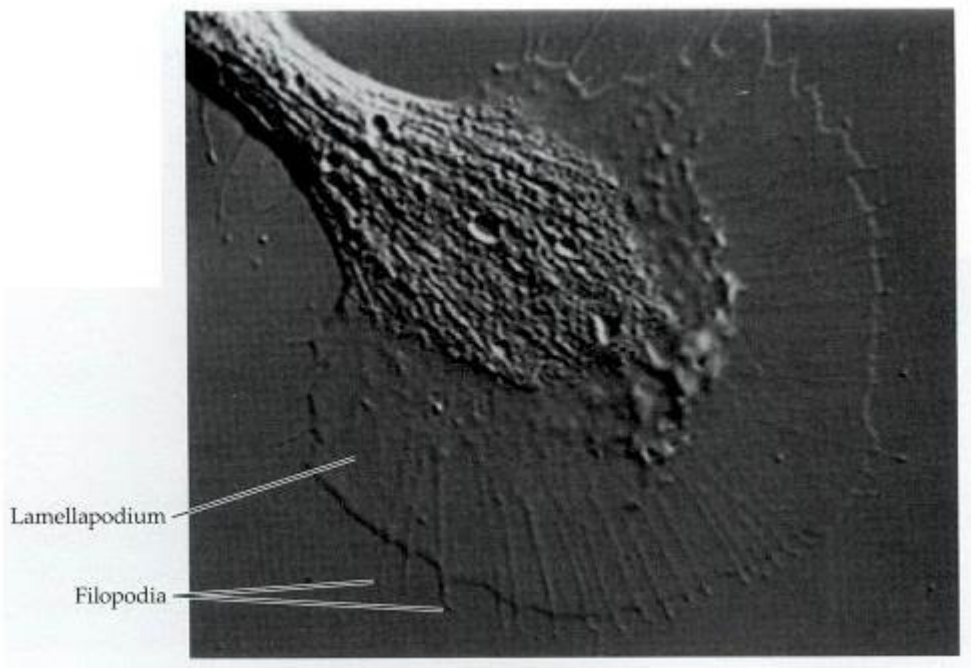

Figure 2.3: Photomicrograph of a growth cone at the tip of a sensory ganglion cell axon. Lamellapodia (flat, sheet like protrusions) and filopodia (long, finger like processes) can be seen arising from the growth cone [19].

Dalby et al [20] explored filopodia sensing by using an array of defined substrates of 35 nm diameter in size. They explained how filopodia probe the shape of a substrate and respond accordingly. For example, in the case of nanotopography, strong perceptions are still noted despite the shape being smaller than the cell. Dalby et al used electron and fluorescent

microscopy on fibroblasts responding to nanopits with 35, 75, and 120 nm diameters, to gain more understanding of what size of feature could be sensed by the filopodia. Nanopits were chosen because unlike many of the surface asperities, they have no distinguishable height for filopodia reaction. This gives an insight into how sensitive filopodia are to their nanoenvironment.

Additional work by [20], the same authors discusses the limit of filopodia sensing by using SEM to image the interactions between 10nm high nano-topography and fibroblast filopodia. In their study, it is clear that a filopodium can be regulated by micro-topography and reacts strongly to nano-scale topography by taking cues from their micro and nanoenvironment. It could also be ascertained that the cells probe the size of the environment using the filopodia, and the filopodia-surface interactions are critical in lowering cell reactions to the extracellular matrix. In order to observe how sensitive the filopodia is to its microenvironment, the study made use of an SEM microscope to observe the cell filopodia and 10 nm high nano-islands, while a fluorescence microscope was used to look at adhesion formation [21]. Their results reveal important characteristics of the filopodia. These characteristics include the use of substrate cues for control of cell growth, development and importantly restore complex tissue function**.**

In a study by J.Meyle et al [22], the researchers discuss surface micro morphology and cellular interactions. They conducted a study using human gingival fibroblasts which are the most abundant cell type in connective tissues. The reactions of filopodia to a regular surface microstructure of 1 μm pitch and 1 μm depth were tested for two days using a TEM. Results show that filopodia exhibits a strong relationship with the topography of a substrate, by either connecting with the groove or following the surface structure.

The work in [23] also discussed the topographical control of a filopodium. The study made use of groove-ridge topographies, aiming to discover the filopodia's response to the topography or to the patterned substratum chemistry formed on the topography. They found that the filopodia stretch receptors are activated when it stretches itself on a substrate. This cytoskeletal activity involves firm adhesions at two or more points to tense the cell (filopodia). This study provides insight on how the filopodia interacts with the surface better.

Work done by K. Anselme et al [24] explained the interaction of filopodia and bacteria with a substrate at the nano-scale, and discussed the effect of size, morphology, organization and separation of nano-features on the filopodia response. This study demonstrates that the filopodia–substrate interactions are second handed by the presence of proteins obtained from biological fluids on the substrate. They studied past histories and developed specific studies, pointing out their relative influences in biological activities: governing cell responses to nanotopography. The study also discussed that different biological molecules could act as cell attachments, most especially as Integrins. Integrins are transmembrane receptors that mediate the attachment between a cell and its surroundings. [24] also discussed works done in the past, in creating differences between the focal complex (adhesion force in small amount measuring 1μm), focal adhesion (adhesion force in large amount measuring from 1 μm to 5 μm) and super –mature adhesions (adhesion force in very large amount measuring less than 5 μm). In accumulation, the surface chemistry on the nanometer scale could be a significant factor in the type of integrin needed by the intermediacy of the absorbed proteins, causing the function of the focal contact. Therefore, patterning on the nanometer scale may have significant role on the organization and the type of focal adhesions formed. The filopodia also respond to topography (substrate) by indirect mechano-transduction, whereby filopodia convert

mechanical cues into chemical messages which arrive at the nucleus through signaling cascades. The mechanical stress leads to activation of several signaling molecules at the adhesion sites. In essence, the relative effect of surface chemistry and topography furthers the understanding between the cell and its substrate in this work.

Finally, Chang-Hwan et al [25] discussed the migrating cell interactions with three dimensions sharp tip nano-topography. The study aimed to discover the effect of substrate nano-topography on migrating cells and 3D parameters, by using two different nano-patterns that have two alternating three-dimensionalities (50-600 nm in nano-structured height). Results showed that the different nano-structures with manageability of pattern, height and shape could act as a means to explain the 3D cell matrix interaction. This enhanced the understanding of the different contact guidance for both filopodia extension and the formation of molecule complex.

2.3 State of the art in modelling filopodia

This section discusses relevant mathematical models that are available in the literature.

Bornschlogl et al [26] studied the dynamics of the filopodia extension and retraction by observing the force exerted by a single filopodium that is contacting an optical trapped bead at its tip. In the experiment [26], a filopodium protruding from a non-migrating cell that is not attached to a substrate was selected as sketched in figure 2.4. The tip of this filopodium was matched to an optically trapped, carboxylated bead (COOH) which caused the filopodium to retract leading to the displacement of the bead. This displacement was relative to the optical trap center. The experiment was repeated to obtain a statistics of the applied force on the filopodium versus the displacement of the optical trap.

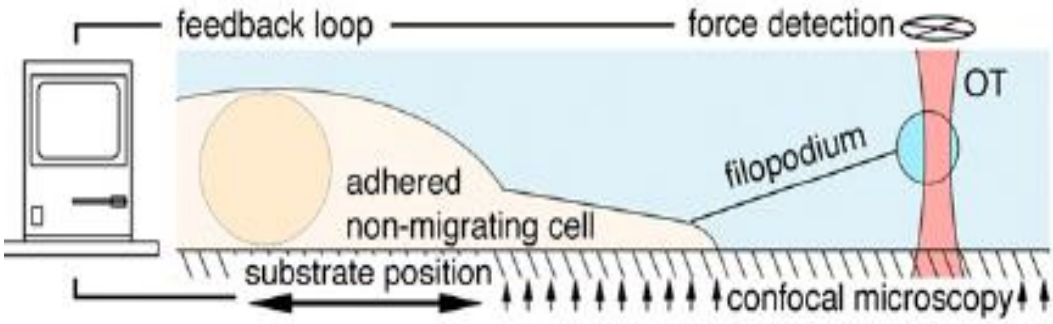

Figure 2.4 Figure extracted from [26]. The filopodium is been anchored from the site of its protrusion by a non- migrating cell.

The filopodia in this experiment [26] was modelled as a lumped parameter model. Essentially, all the parameters in the model were estimated from the experimental data. Figure 2.5 shows the mechanical model of filopodium using lumped parameters.

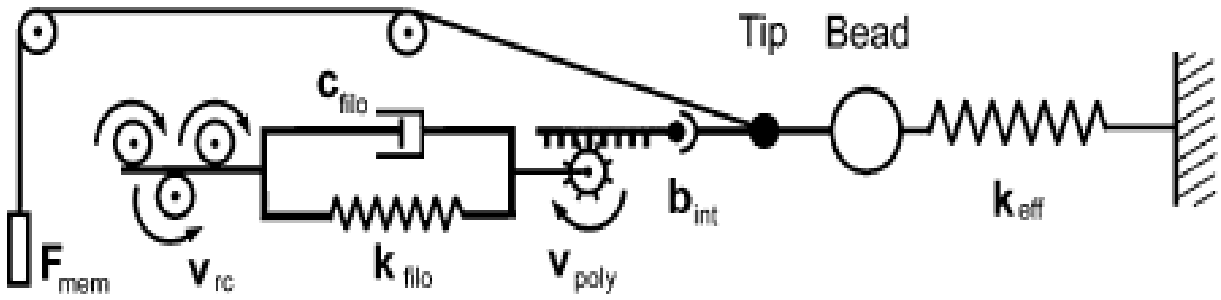

Figure 2.5 Mechanical model for filopodia.

This mechanical model proposed in figure 2.5 describes how a single filopodium exerts a pulling force via its tip. f_{mem} is the force production via the tip from the parallel action of membrane forces and from actin dynamics, V_{rc} is the Cortical retrograde flow couples with high friction to the filopodial actin shaft, modeled as a Kevin–Voigt body with an elastic modulus K_{filo} and a viscosity C_{filo}, V_{poly} is the polymerization at the tip slower than the cortical retrograde flow leads to retraction. Cytoskeletal force transduction can fail due to weak actin–membrane linkage at the tip (b_{int}) and k_{eff} is an elastic force with stiffness controlled by the optical trap is exerted on the bead [26]. It shows that two inward forces are applied by filopodia. This force are the passive force via the membrane and an active cytoskeletal force produced by the retrograde floe in the cortex that is transduced through high frictional coupling the filopodial actin shaft at its base. From this study [26], we want to develop a distributed parameter model that will give a more comprehensive description of the filopodia. Therefore the parameters that will be estimated in this work will be more based on the physics of the system rather than having it kept as a lumped parameter.

Study by Yang et al [27] explained the adhesion of the filopodia to the nanotopography of the substrate. The study includes how the filopodia extends and spreads over the substrate. The study model the filopodia as a rigid beam clamped at one end. This model was chosen because

of the high stiffness of the cross-linked filamentous actin (f-actin). The clamped point indicates the position from which the filopodia protrudes from the cell body as shown in figure 2.6.

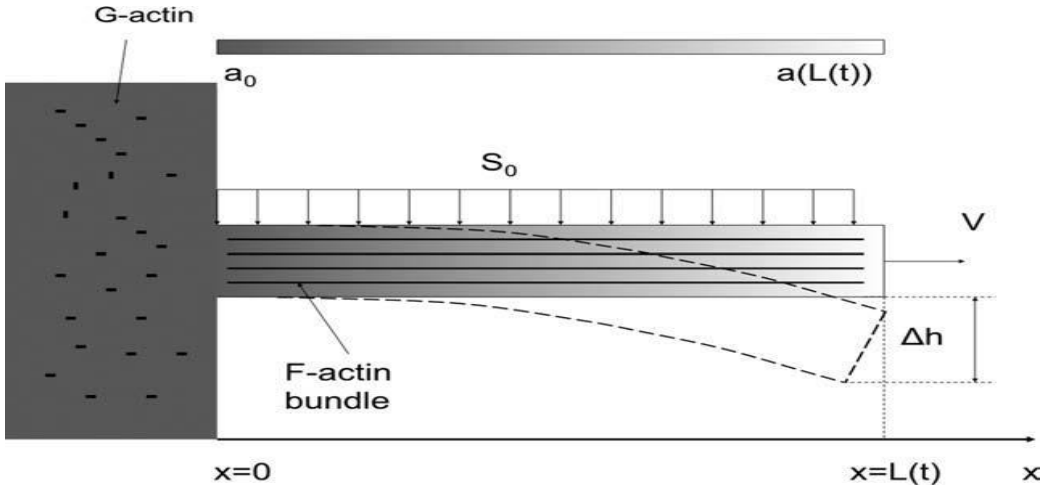

Figure 2.6: Schematic depicting the deflection- diffusion model of filopodia extension [27]

The deflection at the tip of each filopodium is given by [27, 28]

$$\Delta h = \left(\frac{S_0 L^4}{8EI}\right) \tag{2.1}$$

where, S_0 is the uniform attraction exerted on the filopodium, L is the length, E is the elastic module, I is the area moment of inertia, and both combine to form EI the bending stiffness. This refers to the filopodium modeled as a beam.

In [27], the Euler-Bernoulli beam theory has been adopted to model the response of a class of filopodia. Since the beam theory is linear, the analysis applies to systems for which the displacement components u and w (respectively transversal and axial), are small as compared to the beam length L. By considering the abscissa $0 \leq x \leq L$ spanning the initially rectilinear axis of the beam, the small deformation fields are

$$\theta = \frac{du}{dx} = u', \quad \kappa = \frac{d^2u}{dx^2} = u'' = \theta' \tag{2.2}$$

where θ is the rotation of a cross section and κ the curvature of the deflected longitudinal axis [29]. The differential equation governing the static transverse displacement of an Euler-Bernoulli beam is

$$EI\frac{d^4w}{dx^4} = p \tag{2.3}$$

where p is a transverse distributed force, E is the Young's modulus, I is the area moment of inertia of the cross section, x is the abscissa spanning the axis of the filopodia, and w is the trasversal displacement.

The differential equation governing the static axial deformation is

$$EA\frac{d^2u}{dx^2} = \mathfrak{f} \tag{2.4}$$

where A is the cross section area, u is the axial displacement, $\mathfrak{f}$ is the axial distributed force and EA is the axial stiffness. Figure 2.8 shows the images of a filopodium extension on substrate using a SEM.

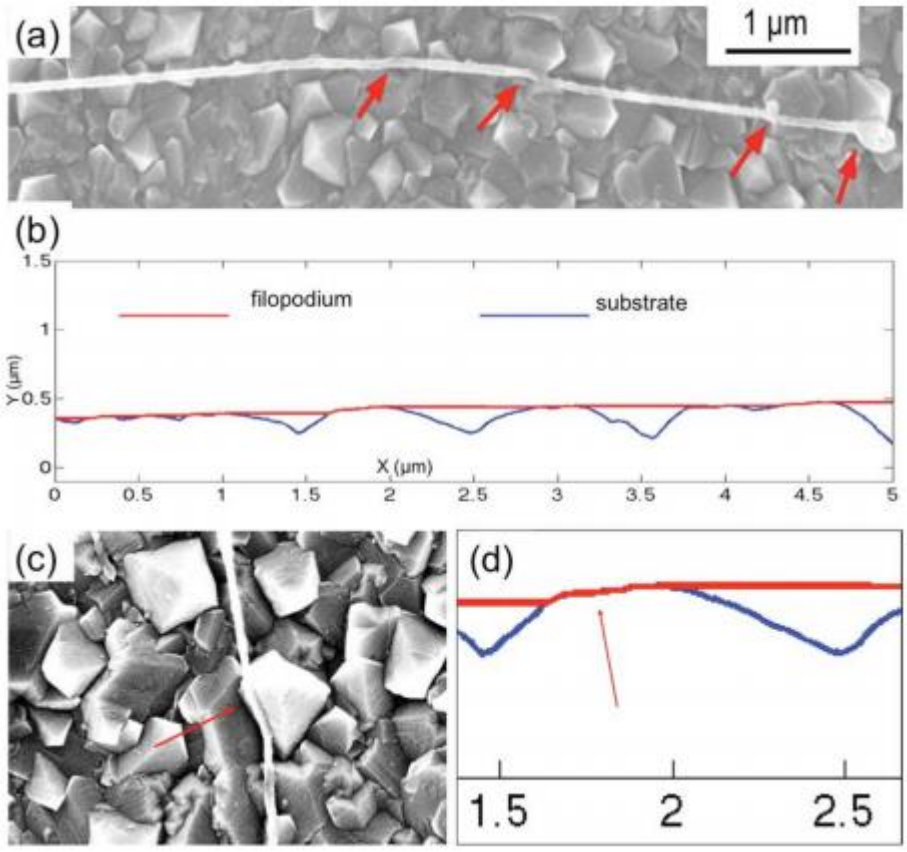

Figure 2.7:(a) SEM images of one osteoblast filopodium extension on submicron crystalline diamond (SMCD), (b) modeling result of filopodia morphology on SMCD, (c) SEM image of a kink in the filopodium formed on the submicron diamond grains, and (d) modeling result showing the kink formed due to substrate topography. Arrows indicate the kinks [27].

Work by Yueheng Lan et al [30], presented model for the growth of a filopodium based on mechanical, physical, and biochemical components. The model provides a complete description of the actin monomer diffusion and polymerization of each individual actin filament under stress. The length distribution of individual filaments in a growing filopodium were investigated and results were shown on how it depends on various physical parameters. The distribution of filament lengths turned out to be narrow, and also the filopodial growth strongly diminished upon increasing retrograde flow[4], this signifies that regulating the

[4] The flow of actin filament back into the body of the cell.

retrograde flow rate would be an extremely effective way to control filopodial extension dynamics. Also, due to the unequal loading of the membrane force[5] among individual filaments, the filopodial length increases as the membrane stress decrease, this was attributed to the larger average polymerization rates. The parameter h was used to represent the average membrane position at the filopodial tip and h_n to represent the length of the nth filament. Since the membrane is supported by the filaments h was then defined as

$$h = max_n(h_n) \tag{2.5}$$

Each actin filament consists of two filaments, which form a right-handed double helix. This resulting structure is very strong. For a given force f, the critical length at which one filament buckles is

$$L_b \approx \frac{\pi}{2}\sqrt{\frac{k_B T L_p}{f}} \tag{2.6}$$

Where L_p is the persistent length, L_b is the buckling length, k_B is the Boltzmann constant. Figure 2.9, the filopodia is divided into compartments with a compartment height I_d starting from the tip.

[5] The internal stress state from the thickness of the filopodium walls.

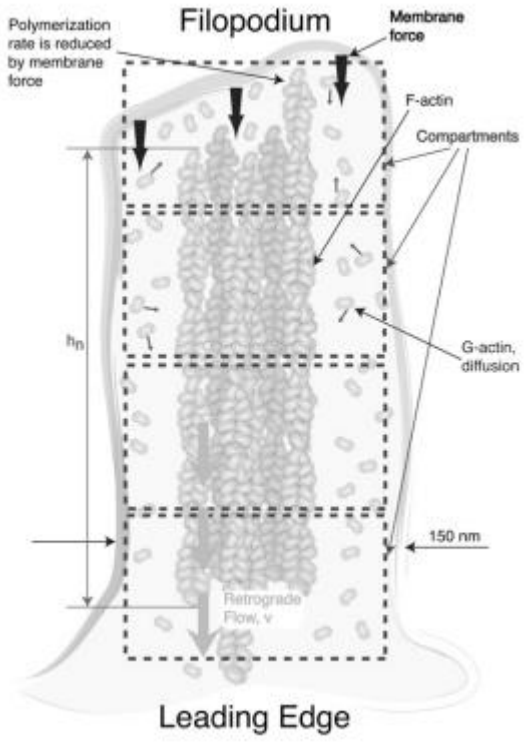

Figure 2.9: Schematic diagram of a matured filopodium where only the most fundamental physicochemical components are shown [30].

The number of actin monomers in a compartment is defined with index I as a_I. The transition rate for one particle moving between neighboring compartments is

$$P_{trans}(I \to I+1) = P_{trans}(I \to I-1) = C_d \tag{2.7}$$

Where C_d is associated to the diffusion constant D, by $C_d = D/I_d^2$. A convenient relation between the loading force f_n and the polymerization rate was calculated to be

$$k_n = k_o exp\left(-\frac{f_n \delta}{k_B T}\right) \tag{2.8}$$

Where k_n is the effective polymerization rate, k_o is the bare rate, δ is the displacement, and f_n is the loading force [31]. Figure 2.10 shows the time evolution of the filopodial lengths obtained from individual trajectories.

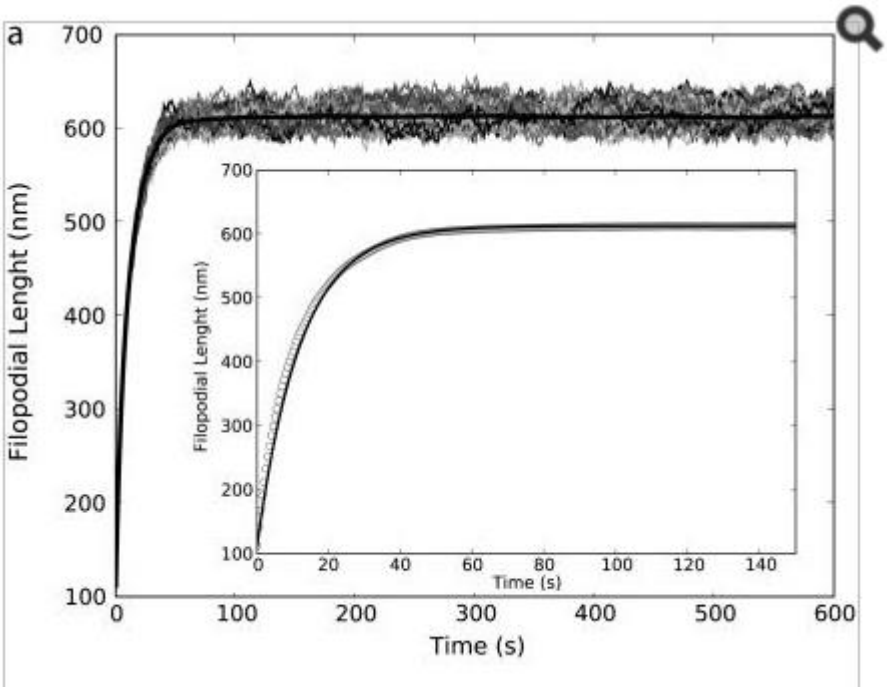

Figure 2.10: Time evolution of the filopodial lengths obtained from individual trajectories. The trajectory average is shown with a thick solid line [30].

Several works have also investigated the physical characteristics of a filopodium such as Oldenbourg et al [31], that studied the movement of filopodia in motile cells using a time-lapse sequence of polarized light images. A simple geometric model for the mechanism of a filopodia protrusion was proposed. From the study by [31], the model was based on two independent motile mechanism, which are the retrograde flow of the f-actin in the lamellipodia and the polymerization of the f-actin at the leading edge. The speeds of lateral movement of actin bundles, and their tilt angle which is in respect to the supervision of the retrograde flow is characterized and incorporated into the model for a filopodium in this thesis.

Further work by Helen M Buettner [32] investigated the dynamic projections from the surface of many motile cell types this includes the filopodia projections, and a simulation model was proposed for the dynamics of the filopodial structure on a nerve growth cone. The model was evaluated to obtain significant relationships between an average filopodial characteristics,

which are normally measured experimental quantities, and the original parameters of individual filopodium dynamics. Its application was to mimic the interaction between a growth cone and its point due to filopodial dynamics. The study by [32, 33] also describes a set of model parameters which includes the rate of filopodial initiation, extension and retraction, filopodial length at maximum extension, and its angular orientation. The mathematical relationship between the model parameters, average filopodial number and length per growth cone were all represented.

In addition, a study by Grimm [34] a mathematical model was developed which is used to investigate the actin dynamics at the leading edge of a crawling cell. This study shows that a filopodium can be modeled as a combination of the extension of the actin network, which relies on the actin filament density. In the next chapter, the model for the filopodia that was used in this study will be presented.

Chapter 3

Mechanical model and estimation of constitutive parameters

3.1 Model overview

This chapter describes a class of mechanical model for a filopodium protrusion. As suggested in [27], strain and strain rate dependency should be included in the constitutive model to describe the system's response. Therefore in this work, we consider a viscoelastic response. Viscoelastic response is frequently used as a probe in tissue science, because it is sensitive to material's chemistry and microstructure. This concept and techniques are vital here, to reveal how linear viscoelasticity can be integrated into the general theory of mechanics of materials, so that structures containing viscoelastic components can be premeditated and analyzed. When subjected to an applied stress, cells deforms by either the length or angle of the applied force. This small motion happens very quickly. A von Karman relation which has a coupled form in the strain tensors, was also introduced to couple the bending and elongation equation of the system.

3.2 Kelvin Voigt viscoelastic model

The lumped parameters mechanical system associated to this model consists of a spring and a dashpot in parallel configuration as shown in figure 3.1. Subscripts 's' and 'd' denote the spring and dashpot respectively. The total stress σ applied to the entire system produces stresses σ_s and $\sigma_d$in the spring and the dashpot [35].

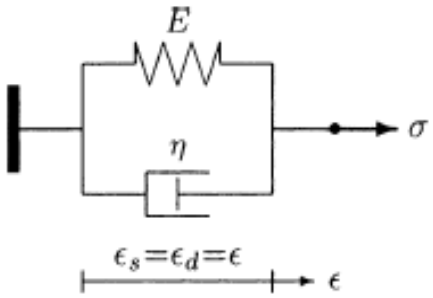

Figure 3.1. Kelvin Voigt model [35].

The total stress applied to the system is therefore given by

$$\sigma = \sigma_s + \sigma_d \tag{3.1}$$

On the other hand, since the spring and the dashpot are in parallel and deform equally, the total strain ε of the system is equal to the strains ε_s and $\varepsilon_{d.}$ of the spring and the dashpot respectively,

$$\varepsilon = \varepsilon_s = \varepsilon_{d.} \tag{3.2}$$

The stress strain relationships for the spring and the dashpot are

$$\sigma_s = E\varepsilon_s \tag{3.3}$$

$$\sigma_d = \eta\dot{\varepsilon}_{d.} \tag{3.4}$$

By substituting equations (3.3) and (3.4) into equation (3.1) we have:

$$\sigma = E\varepsilon_s + \eta\dot{\varepsilon}_d \tag{3.5}$$

From equation (3.2), $\varepsilon = \varepsilon_s = \varepsilon_{d.}$ so,

$$\sigma = E\varepsilon + \eta\frac{d\varepsilon}{dt} \tag{3.6}$$

Then by defining differential operators,

$$P(\sigma) = 1 \tag{3.7a}$$

$$S(\varepsilon) = E + \eta \frac{\mathrm{d}\varepsilon}{\mathrm{dt}} \tag{3.7b}$$

the equation (3.6) can be rewritten in operator form as,

$$P(\sigma) = S(\varepsilon) \tag{3.8}$$

3.3 Von Karman Kinematics

The von Karman beam is introduced in our simulation, to couple the bending and elongation equation of the system for the case study in chapter 4. Therefore the Green-Saint-Venant strain in Cartesian coordinates is given by

$$\varepsilon_{ij} = \frac{1}{2}\left(\frac{\partial u_i}{\partial x_j} + \frac{\partial u_j}{\partial x_i} + \frac{\partial u_k}{\partial x_i}\frac{\partial u_k}{\partial x_j}\right) \tag{3.9}$$

where indexes i,j=1,2,3 refer to coordinate directions, considering u_x , u_y and u_z as displacements of the beam at any point in the x, y, and z direction, respectively. Substitution displacement fields into (3.11), the expressions for the strain displacement due to von Karman, in $x - z$ plane of mid-plane, can be rewritten as,

$$\varepsilon_{xx} = \frac{\partial u_x}{\partial x} + \frac{1}{2}\left[\left(\frac{\partial u_x}{\partial x}\right)^2 + \left(\frac{\partial u_y}{\partial x}\right)^2 + \left(\frac{\partial u_z}{\partial x}\right)^2\right] \tag{3.10}$$

considering u, v, and w as displacements of the middle surface respectively in the x, y, and z direction, and Kirchhoff's hypothesis, the displacement yields are expressed as,

$$u_x = u - z\frac{dw}{dx} \qquad u_y = 0 \qquad u_z = w \tag{3.11}$$

and therefore the strain (3.11) can be rewritten as,

$$\varepsilon = \frac{\partial u}{\partial x} + \frac{1}{2}\left[\left(\frac{\partial w}{\partial x}\right)^2 + \left(\frac{\partial u}{\partial x}\right)^2\right] - z\left(1 + \frac{\partial u}{\partial x}\right)\frac{\partial^2 w}{\partial x^2} + \frac{z^2}{2}\left(\frac{\partial^2 w}{\partial x^2}\right)^2 \tag{3.12}$$

where the subscript of ε_{xx} is dropped to simplify the equation. Then the resultant normal force and moment of the beam are,

$$N(x,t) = \int_A \sigma dA = \int_A E\varepsilon dA \tag{3.13a}$$

$$M(x,t) = -\int_A \sigma z dA = -\int_A E\varepsilon z dA \tag{3.13b}$$

Finally, the constitutive equations for membrane force and bending moment in terms of displacement can be derived as,

$$N(x,t) = \frac{1}{2}\left[A\left(\left(\frac{\partial u}{\partial x}\right)^2 + 2\frac{\partial u}{\partial x} + \left(\frac{\partial w}{\partial x}\right)^2\right) + EI\left(\frac{\partial^2 w}{\partial x}\right)^2\right] \tag{3.14a}$$

$$M(x,t) = EI\frac{\partial^2 w}{\partial x} + EI\frac{\partial u \partial^2 w}{\partial x \partial x^2} \tag{3.14b}$$

where, $\int_A z dA = 0$ and $I = \int_A z^2 dA$, since the neutral axis passes through centroid of the beam.

3.4 Von Karman Viscoelasticity

Considering differential operators in (3.7a), the viscoelastic membrane force and bending moment in (3.14) can be rewritten in operator form as,

$$P\big(N(x,t)\big) = \int_A P(\sigma) dA = \int_A ES(\varepsilon) dA \tag{3.15a}$$

$$P\big(M(x,t)\big) = -\int_A P(\sigma) z dA = -\int_A ES(\varepsilon) z dA \tag{3.15b}$$

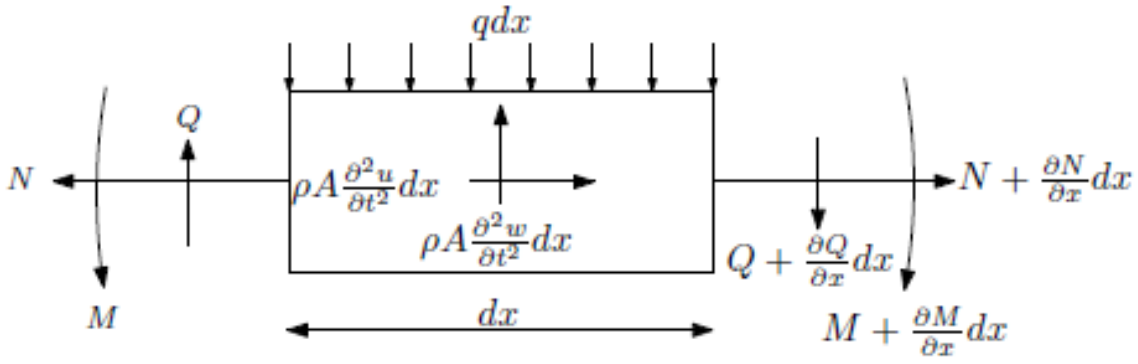

Figure 3.2 Schematic depicting the force equilibrium of a deformed beam element of length dx.

Then by applying system stain-displacement relation in (3.12), and substituting it into (3.15), the constitutive relations for membrane force and bending moment in a viscoelastic von Karman beam can be expressed as,

$$P\big(N(x,t)\big) = \left(\frac{E}{2} + \frac{\eta}{2}\frac{\partial}{\partial t}\right)\left[A\left(\left(\frac{\partial u}{\partial x}\right)^2 + 2\frac{\partial u}{\partial x} + \left(\frac{\partial w}{\partial x}\right)^2\right) + I\left(\frac{\partial^2 w}{\partial x}\right)^2\right] \tag{3.16a}$$

$$P\big(M(x,t)\big) = \left(EI + I\eta\frac{\partial}{\partial t}\right)\left[\frac{\partial^2 w}{\partial x}\left(1 + \frac{\partial u}{\partial x}\right)\right] \tag{3.16b}$$

3.5 Equation of Motion

Figure 3.2 shows the force equilibrium with a deformed beam element of length dx, in which $q(x,t)$ is the applied transverse weight force, $Q(x,t)$ is the internal shear force, $N(x,t)$ is the internal membrane force, $M(x,t)$ is the internal moment, ρ is the mass of the beam element. Then the balances of forces in the vertical and axial directions are

$$\left(N(x,t) + \frac{\partial N(x,t)}{\partial x}\right) - N(x,t) = \rho A\frac{\partial^2 u(x,t)}{\partial t^2} \tag{3.17a}$$

$$q(x,t) + \left(Q(x,t) + \frac{\partial Q(x,t)}{\partial x}\right) - Q(x,t) = \rho A \frac{\partial^2 w(x,t)}{\partial t^2} \tag{3.17b}$$

Considering sum of moments about the center of the beam element and neglecting rotatory inertia,

$$Q(x,t) = \frac{\partial M(x,t)}{\partial x} + N \frac{\partial w(x,t)}{\partial x} \tag{3.18}$$

Substituting (3.18) into (3.17b) and applying the differential operator (3.10), the equation of motion for a von Karman viscoelastic beam can be expressed as,

$$\rho A \frac{\partial^2 u(x,t)}{\partial t^2} - P \frac{\partial N(x,t)}{\partial x} = 0 \tag{3.19a}$$

$$\rho A \frac{\partial^2 w(x,t)}{\partial t^2} - P \left(\frac{\partial^2 M(x,t)}{\partial x^2} + N \frac{\partial w(x,t)}{\partial x^2}\right) = q(x,t) \tag{3.19b}$$

The governing equation for a viscoelastic von Karman beam are expressed by the following coupled partial differential equations

$$\rho A \frac{\partial^2 u(x,t)}{\partial t^2} - \frac{1}{2}\left(E \frac{\partial}{\partial x} + \eta \frac{\partial^2}{\partial t \partial x}\right)\left[A\left(\left(\frac{\partial u}{\partial x}\right)^2 + 2\frac{\partial u}{\partial x} + \left(\frac{\partial w}{\partial x}\right)^2\right) + I\left(\frac{\partial^2 w}{\partial x^2}\right)^2\right] = 0 \tag{3.20a}$$

$$\rho A \frac{\partial^2 w(x,t)}{\partial t^2} - I\left(E \frac{\partial^2}{\partial x^2} + \eta \frac{\partial^3}{\partial t \partial x^2}\right)\left[\frac{\partial^2 w}{\partial x^2}\left(1 + \frac{\partial u}{\partial x}\right)\right] - \frac{1}{2}\left(E + \eta \frac{\partial}{\partial t}\right)\left[A\left(\left(\frac{\partial u}{\partial x}\right)^2 + 2\frac{\partial u}{\partial x} + \left(\frac{\partial w}{\partial x}\right)^2\right) + I\left(\frac{\partial^2 w}{\partial x^2}\right)^2\right]\frac{\partial^2 w}{\partial x^2} = q(x,t) \tag{3.20b}$$

3.6 Linear Viscoelastic beam

The linear viscoelastic beam can be suggested to predict the response of a filopodium. Therefore a constitutive model for the body of a filopodium, and the general stress-strain equation for bending, the governing equation can be rewritten as

$$P(q) = S(-I\eta \frac{\partial^5 w}{\partial t \partial x^4} - IE \frac{\partial^4 w}{\partial x^4}) \tag{3.21}$$

where I is the area moment of inertia, S and P are functions, presented in equation (3.22), and (3.23). Stress response $P(w)$ is equal to strain response of the model with respect to applied force, q. So the strain response of the model for bending can be presented as,

$$S(w) = \eta \frac{\partial w}{\partial t} + E \tag{3.22}$$

where E is the Young Modulus, q and f are defined as the distributed force in equation (3.23) and (3.26). We consider the distributed force q through the length of the filopodium as

$$q = -\rho A \frac{\partial^2 w}{\partial t^2} + \overline{q}(x) \tag{3.23}$$

where ρ is the density of the filopodium, $\overline{q}(x)$ is the applied force and A is the area of the filopodium.

The general equation for the bending of a filopodium can then be expressed as

$$I\eta \frac{\partial^5 w}{\partial t \partial x^4} - IE \frac{\partial^4 w}{\partial x^4} + \rho A \frac{\partial^2 w}{\partial t^2} = q \tag{3.24}$$

For the elongation of a filopodium, the governing equation can be rewritten as

$$P(f) = S(A\eta \frac{\partial^3 u}{\partial t \partial x^2} - AE \frac{\partial^2 u}{\partial x^2}) \tag{3.25}$$

where A is the area, S are functions, presented in equation (3.22). Considering the distributed force through the length of the filopodium as

$$f = -\rho A \frac{\partial^2 u}{\partial t^2} + \overline{f}(x) \tag{3.26}$$

where $\overline{f}(x)$ is the applied force.

The general equation for the elongation of a filopodium can then be expressed as

$$A\eta \frac{\partial^3 u}{\partial t \partial x^2} - AE \frac{\partial^2 u}{\partial x^2} + \rho A \frac{\partial^2 u}{\partial t^2} = f \tag{3.27}$$

3.7 Estimation of constitutive parameters

In other to simulate the system, there is need to estimate linear viscoelastic material parameters appearing in the governing equations by virtue of the constitutive assumptions. The estimation of these parameters is crucial for the accuracy of the predictions of the model, and it is particularly challenging because beam theory parameters have to be identified and estimated from a body of literature that is mainly focused on experimental work not directly targeting this class of models. The characterizations of parameters were based on the material and geometry of the structure of the filopodia as described in technical literature. Experimental results from [36] were also used to estimate the elastic and viscoelastic coefficient. Predictions from these models are compared and discussed.

3.7.1 Estimation of Young's modulus (E)

Xiong et al [37], studied the topography and nanomechanics of live and fixed neuronal growth cones. These live and fixed neuronal growth cones are the physical condition in which the motile structures located at the end of axons are present. Axons are long slender projection of a nerve cell that convert extracellular guidance information into directional movements. In the study, AFM was used to observe the P domain, C domain, and the T zone of a live Aplysia growth cone. The P (Peripheral) domain consists of the lamellipodial veils that are separated by the filopodia. The T (Transition) zone consists of actin bundles called ruffles or intrapodia. The C (Central) domain consists of microtubules of the live Aplysia growth cone. The height of these regions was computed from the AFM images while the nano-indentation measurements produced Young's modulus of the P domain, C domain, and the T zone. Figure 3.4 shows the schematic of the growth cone cytoplasmic and the cytoskeletal organization.

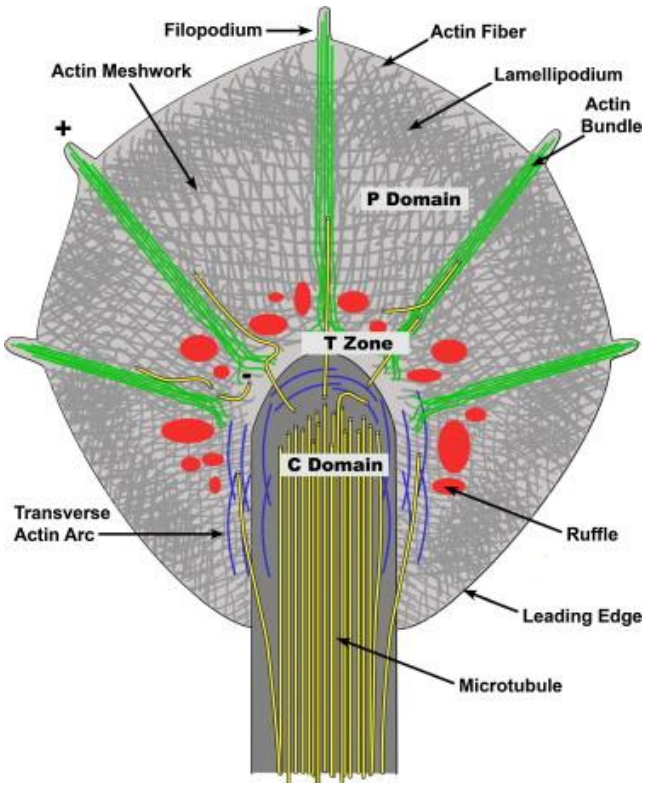

Figure 3.4: Schematic of growth cone cytoplasmic and cytoskeletal organization [37]

The study provides the mechanical properties of the growth cones (lamellipodia and filopodia bundles). The value of the Young's modulus E of a filopodium is reported to be between 20-40 kPa. Estimates from this work are summarized in the Table 1.

Table 1: Mechanical properties of different growth cones [37]

Fixed Growth Cones			Live Growth Cones			
	Young's Modulus (kPa)		Young's Modulus (kPa)			
Domain	Range	Average	Range	Average	SEM	n
P domain Lamellipodia	85-135	110	10-25	16.7	1.05	113
P domain Filopodia	-	-	20-40	29.8	1.35	71
T zone ruffles	176-225	200	7-23	15.7	3.5	194
C domain	45-95	70	3-7	5.7	0.5	42

C, central; P, peripheral; SEM, standard error of mean; T, transition, n, number of measurement

3.8 Estimation of the weight of a filopodium

As stated in Chapter 1, a filopodium consists of actin filaments (< 10 actin filaments), and these actin filaments are made up of actin molecules. It is therefore possible to estimate the weight of a filopodium based on this knowledge of its sub-units [38].

The molecular weight of an actin molecule is first determined. This molecular weight is obtained from [39] where the molecular weight of one actin molecule is estimated to be 42 kDa. The 42kDa (kilodalton) gives a molecular weight of $6.8414\times\ 10^{-25}\ g\mu m/s^2$.

Based on the same study [39], the length of an actin molecule is estimated to be 5.5nm, which converted to micrometers gives $0.0055\ \mu m$.

From equation (3.28) the weight of a filopodium is therefore expressed as a function of the

length L and the number of filaments m by

$$W = 6.8414\times\ 10^{-25} \times \frac{L}{0.0055} \times m \tag{3.28}$$

3.9 Geometry of the cross section

The geometry of the cross section is crucial to determine the axial and the bending stiffness. The geometry is estimated based on published work from which the relevant information could be extrapolated. Mattila [4, 6] studied the mechanism underlying the initiation and dynamics of neuronal filopodia. The study made use of Atomic Force Microscopy (AFM) to extract quantitative information on the mechanical and volumetric properties of cells. The diameter of a filopodium is estimated to be in the range of 100 – 300 nm approximately.

By assuming circular cross section, the area is calculated as

$$A = \frac{\pi d^2}{4} \tag{3.29}$$

By using the estimated diameter we can also compute the area moment of inertia of the cross section as

$$I = \frac{\pi d^4}{64} \tag{3.30}$$

By using the estimated Young's modulus of the peripheral domain of the filopodium in Table 1 and geometry of the cross section from equation (3.29) and (3.30), we obtain the values of axial and bending stiffness in Tables 2 and 3.

Table 2: Axial stiffness of a filopodium using the geometry and material parameters when the diameter is 200nm.

Young's modulus E (kPa)	Area A (m^2)	Axial stiffness EA (N)
20	$3.1415 \cdot 10^{-14}$	$6.2383 \cdot 10^{-10}$
30	$3.1415 \cdot 10^{-14}$	$9.4248 \cdot 10^{-10}$
40	$3.1415 \cdot 10^{-14}$	$1.2566 \cdot 10^{-9}$

Table 3: Bending stiffness of a filopodium using the geometry and material parameters when the diameter is 200nm

Young's modulus E (kPa)	Area moment of inertia I (μm^4)	Bending stiffness EI (N/m)
20	$7.8539 \cdot 10^{-5}$	$1.5708 \cdot 10^{-24}$
30	$7.8539 \cdot 10^{-5}$	$2.3562 \cdot 10^{-24}$
40	$7.8539 \cdot 10^{-5}$	$3.1416 \cdot 10^{-24}$

3.10 Estimation of viscoelastic parameters

We estimated the viscoelastic parameters from an experimental work by [36]. The mechanical properties for the Kelvin–Voigt viscoelastic model are reported for elastic coefficient $E = 725\ N\ m^{-1}$ and viscoelastic coefficient $\eta = 8500\ N/ms$.

Chapter 4

Results and Discussion

4.1 Overview

The present chapter shows the model validation and results, obtained from the numerical simulations and comparison with the experimental results of Alexandra et al [36]. A case describing a filopodium crossing an asperity as shown in figure 4.6 is studied numerically. We considered a filopodium with initial length $l = 24\,\mu m$, density$\rho = 1025\ kg/m^3$, viscoelastic coefficient $\eta = 8700\ N/m^2 s$, weight $= 55\ kDa$, cross section A = 5.72555 $pico\ m^2$, and elastic coefficient E = 725 N/m^2. The viscoelastic coefficient η, elastic coefficient E and density ρ were obtained from the literature in [36] as explained in chapter 3.

4.2 Model Validation

Filopodia are viscoelastic dynamic plasma membranes. The dynamic and biochemical responses of a filopodium can be described by a viscoelastic response [26]. Filopodia viscoelastic properties can be estimated and analyzed using the constitutive law of rheological mechanics. Therefore, the viscoelastic properties of filopodia can be identified through some routine experimental tests like creep and relaxation [40].

The density, length and area of a filopodium is reported in [10, 6] to be respectively 1025 [$kg\backslash m^3$], $24 \times 10^{-6}\ m$ and $1.35^2\pi \times 10^{-12}\ mm$. The mechanical properties for the Kelvin–Voigt viscoelastic model are $E = 725\ N\ m^{-1}$ and $\eta = 8500\ N/ms$ which are obtained from [36].

We used the linear viscoelastic beam will a Kelvin Voigt response which is a distributed system to reproduce the experimental result obtained by [36], which studied the mechanical response

of a predeformed filopodium to external forces. These external forces are exerted by magnetic tweezers in a reflection interference contrast microscopy as shown in the figure 4.1.

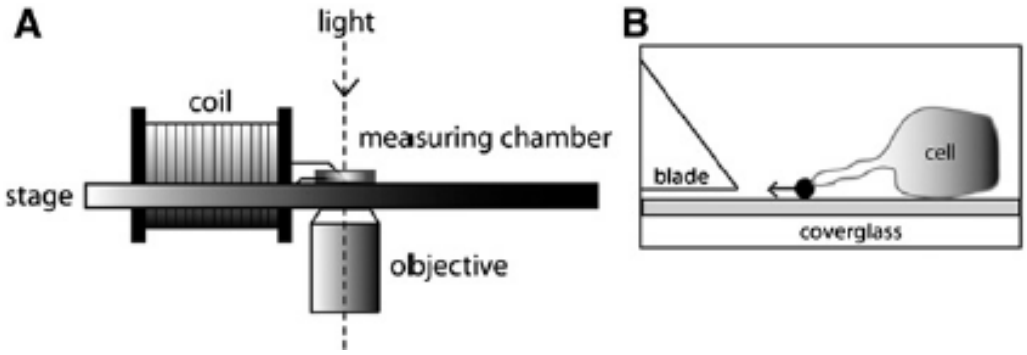

Figure 4.1. Experimental setup of magnetic tweezers. (A) Schematic view of the magnetic tweezers setup. (B)Cartoon of the inside of the measuring chamber with a macrophage exposing a filopodium that is attached to the magnetic bead. The arrow indicates the direction of force [36].

In order to relate the time evolution of a force-induced elongation to the mechanical properties of a filopodia, [36] studied the viscoelastic response of the filopodium protrusions to single force pulses and staircase-like pulse sequences. In the experiment for single-impulse, force amplitudes (f_0) between 0.02 and 0.6 nN lasting 15–30 seconds were applied. This produces a displacement-time diagram for a single impulse of 0.3 nN and 16 seconds duration as shown in figure 4.2.

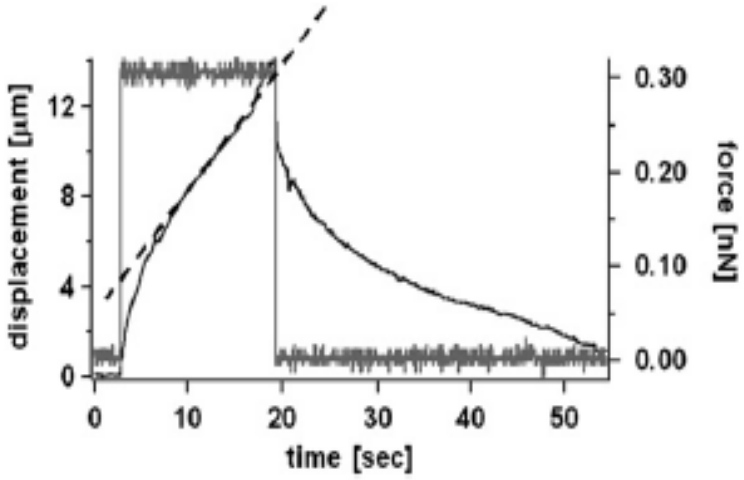

Figure 4.2 A viscoelastic response of filopodia. A typical elongation versus- time plot evoked by a single force pulse (gray line). The displacement $u(t)$ (black line) consists of an initial viscoelastic response followed by a linear flow regime (characterized by straight line , which defines the average elongation velocity, <v> (dashed line) [36].

We used independently obtained parameters which were published in experimental result by [36], but obtained from another experiment data, to see if our response and experimental response fit. The material and geometry parameters of the filopodium were obtained from the details given in the experiment [10, 6]. We compared the experiment measurements to the distributed model, which was obtained using the linear viscoelastic beam in the same plot as shown in Figure 4.3.

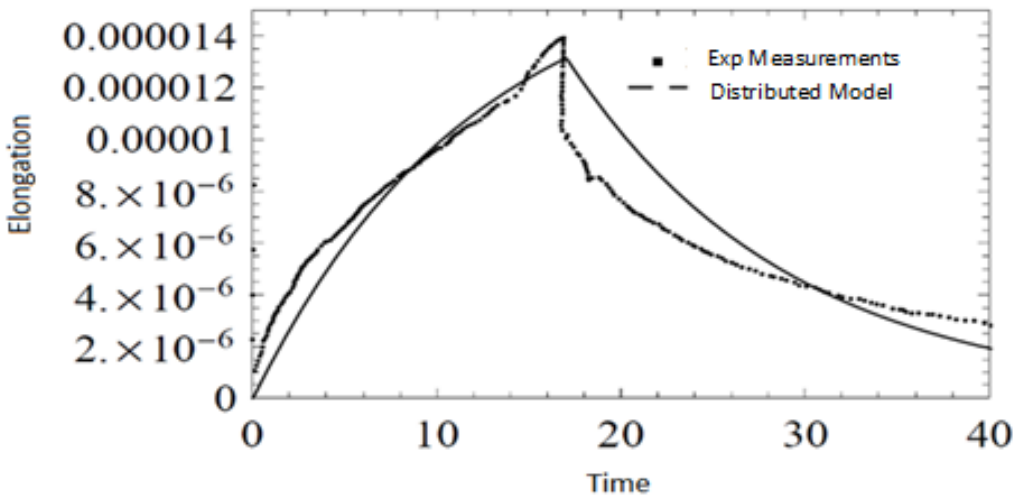

Figure 4.3 Comparison between the fitted model and the experimental measurements.

From figure 4.3, we can say that the viscoelastic beam with Kelvin Voigt material response is reliable in predicting the viscoelastic response of an elongated filopodia, and can then be used to show other responses of the filopodia.

4.3 Case study: filopodia crossing over an asperity.

4.3.1 Overview

This section is dedicated to the description of typical interaction between filopodia protrusions and its micro-environment from the perspective of the adopted viscoelastic model. These interactions have been experimentally studied as they generally affect the overall growth and protrusion processes of cells on substrates. Therefore it is relevant to be able to describe such processes with the simple model adopted in this work, and eventually be able to predict related bio-mechanic effects. This case describe how filopodia react from a mechanical point of view to external conditions which can impact its protrusion. Different boundary conditions are set depending on the physical system one wants to model. Filopodia protrusions are assumed to have a viscoelastic response, which is described by the Kelvin Voigt model.

4.3.2 Filopodium crossing an asperity

Numerous studies have discussed some of the factors that affect the cell- substrate relationship. These factors include environmental factors [41] and the limit of filopodia sensing on different substrate sizes [21, 42, 24, 43, 44]. In addition, we try to study a case of a filopodium crossing over an asperity. An image of a filopodium crossing an asperity is shown figure 4.5.

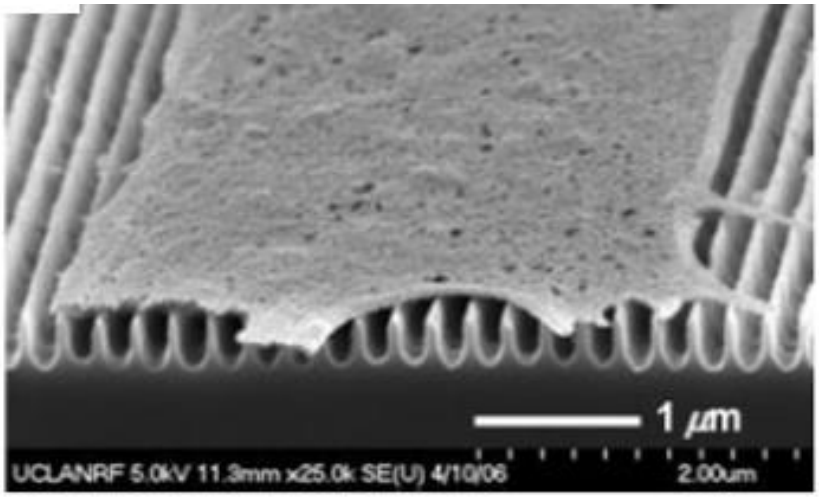

Figure 4.4: SEM image of Filopodia crossing an asperity [44, 25].

Considering a forward motion with tip elongation rate v, for a filopodia on asperity surface (see Fig. 4.6) boundary and initial conditions are:

$$u(0,t) = 0, \frac{\partial u}{\partial t}(L,t) = v$$

$$w(x,0) = 0, \frac{\partial w}{\partial t}(0,t) = 0$$

$$u(x,0) = 0, w(x,0) = 0$$

$$P\big(M(L,t)\big) = 0, P\left(\frac{\partial M(L,t)}{\partial x}\right) = 0$$

4.4 Result for the Simulation of a filopodium crossing an asperity

We implemented the coupled equation in (3.20) for the bending and elongation von Karman viscoelastic beam. This was achieved by the NDSolve routine in Mathematica, which uses the Runge-Kutta time integration scheme in the finite elements method. Considering a given elongation rate v and a defined gap δ_o between the filopodium and the substrate, we sought to obtain the maximum width δ a filopodium can cross as sketched in figure 4.6. This means the maximum distance the stiffness of the filopodia can overcomes it's weight that causes it to bend. The value of the parameter δ is determined by stopping the simulation when the bending equals the gap δ_o.

This is important because it explains the distance sufficient to overcome the bending caused by the weight, when a filopodium is crossing an asperity. In other words when a filopodium is crossing over an asperity, there is a weight acting on it from the influence of gravity and over a certain distance this weight will cause the filopodium to bend. There is also a stiffness from the filopodium, so if the distance is not that large, we are expecting the filopodia to cross over an asperity even if the two parts are of the same height, because at a certain distance the stiffness is sufficient to overcome the weight. This is to say that the bending caused by the weight can be negligible within some certain distance.

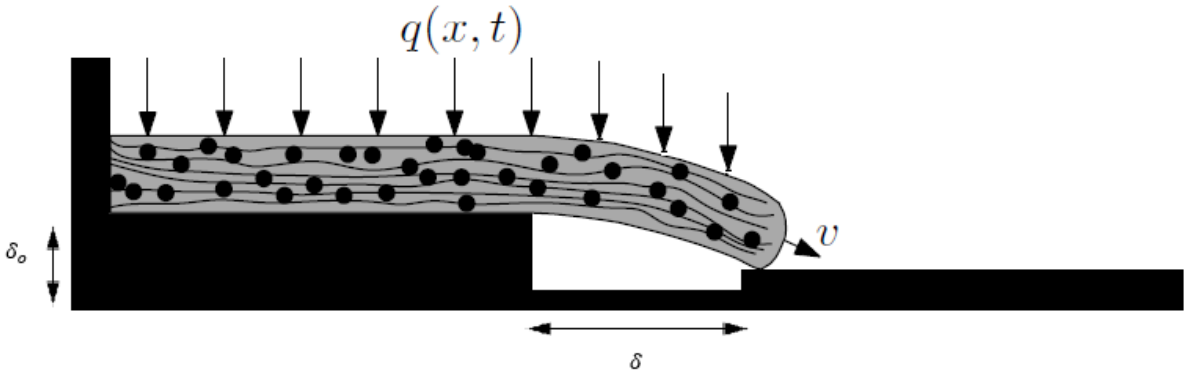

Figure 4.5: Schematic model of filopodia extension

For a case study, the gap between the filopodium and the substrate is assumed to be $\delta_o = 0.001\mu m$. We ran the simulation for an elongation rate $v = 0.1\mu m/s$ and stopped the simulation when the bending was equal to the gap between the filopodium and the substrate δ_o. We obtained an elongation of 2.9 μm. These steps were also repeated for an elongation rate $v =$ 0.15 $\mu m/s$, 0.2 $\mu m/s$, 0.25 $\mu m/s$, 0.3 $\mu m/s$, 0.35 $\mu m/s$ and 0.4 $\mu m/s$ and resulted in an elongations of $\delta =$ 4.35 μm , 5.8 μm , 7.25 μm , 8.7 μm , 10.15 μm and 11.6 μm respectively. Figure 4.6 shows the results obtained for the elongation δ of a filopodium protrusion, for different elongation rate v on the substrate over an asperity.

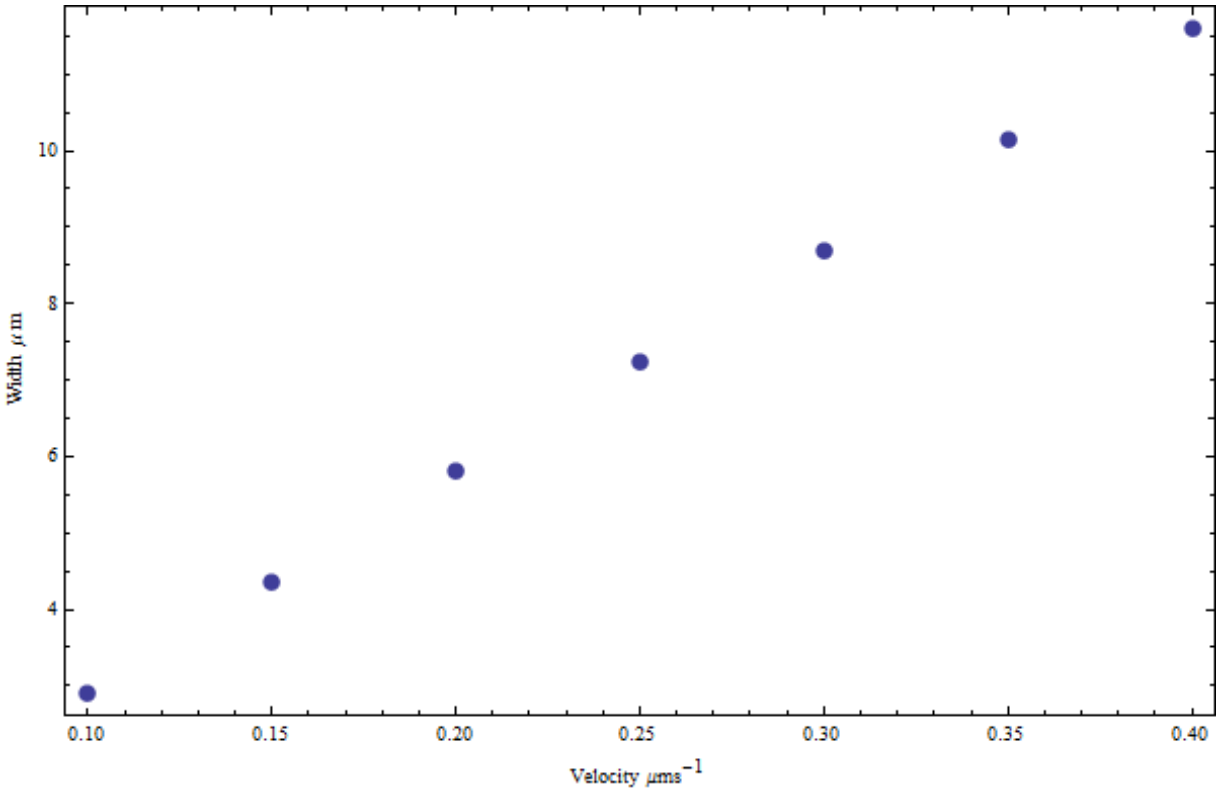

Figure 4.6: Relationship between the velocity and the width.

Figure 4.6 shows that increasing elongation rate v at the tip of the filopodium causes more elongation δ in the mechanism. It shows that at a certain range of velocities there is a linear relationship between the gaps. It also suggests that a filopodium protrusion will not be interrupted for a width $< 2.9\,\mu m$ for an elongation rate $v = 0.1\,\mu m/s$, or for a width $< 5.8\,\mu m$ for an elongation rate $v = 0.2\,\mu m/s$, or for a width $< 8.7\,\mu m$ for an elongation rate $v = 0.3\,\mu m/s$.

For better understanding of the filopodia response in different situations, we showed the effect of change in gap between the filopodium and the substrate

4.4.1 Effect of change in gap between the filopodium and the substrate.

In this case we ran the simulation for gaps δ_o = 0.003, 0.006, 0.010, 0.014, 0.0177 and 0.021 μm with constant elongation rate v = 0.1 $\mu m/s$. We stopped the simulation when the bending was equal to these gaps δ_o. Figure 4.8 shows the result obtained for the elongation δ, for example, it shows that if the gap between the two parts is $> 0.0005\ \mu m$, the filopodium will cross over provide the maximum width between the two parts is $\leq\ 1\ \mu m$.

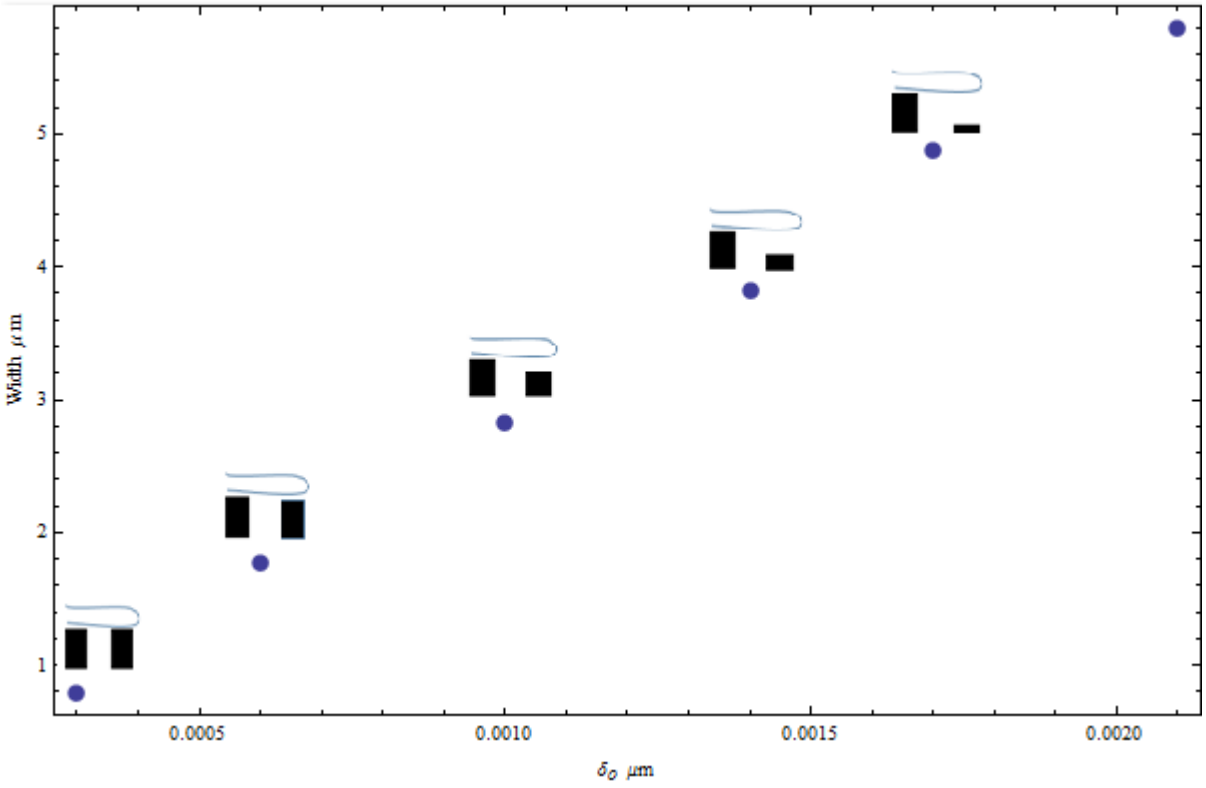

Figure 4.7 Relationship between the elongation and gap δ_o

This result matches the experimental conditions in figure 4.8. This data can be applied for designing biomechanical surfaces which can be tested for different experiment.

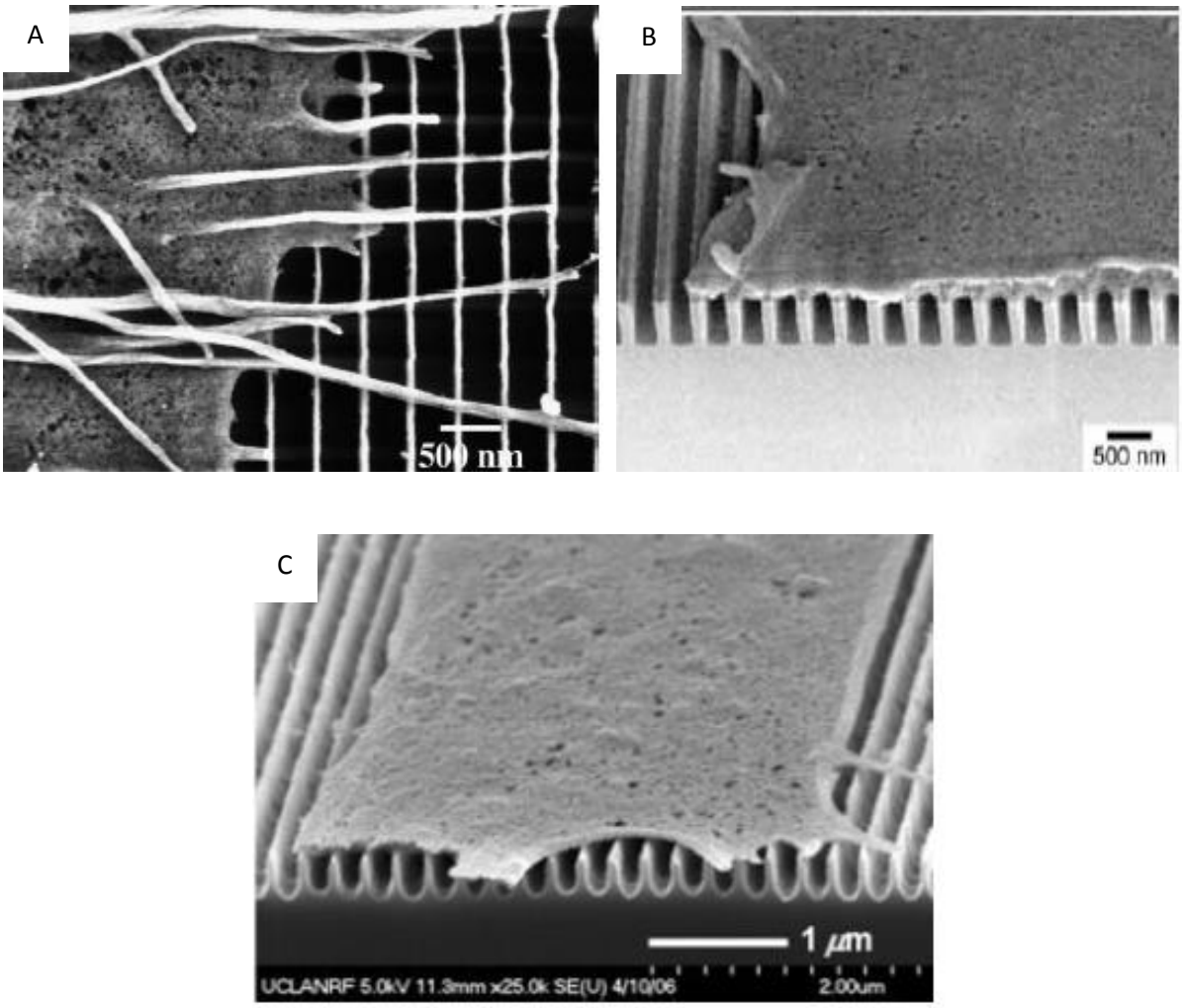

Figure 4.8: SEM images of a filopodium crossing over an asperity [44, 25].

Figure 4.8 shows the SEM images of a filopodium crossing over an asperity. Figure 4.8A and 4.8B, shows that a filopodium protruding over a gap of width $= 500\ nm$, while figure 4.8C shows that a filopodium protruding over a gap of width $= 1\ um$. These quantities are in agreement with numerical results shown in showed in figure 4.6 and 4.7, and suggest that the viscoelastic beam model could be used to predict this class of interactions.

In conclusion the mathematical model in this work, is sufficient to predict the filopodia protrusion. In the next chapter, we summarize and concluded the works be done.

Chapter 5

Summary and Conclusion

In this work, mathematical simulation for filopodial protrusion were modelled using the linear viscoelastic model with Kelvin Voigt material response. The von Karman viscoelastic beam model was also introduced to couple the bending and elongation equation for a filopodium protrusion. The viscoelastic model was used because a filopodium exhibits a viscous and elastic behaviour meaning it has a time dependant strain.

For the accurate prediction of the system, a certain number of beam parameters were needed to be estimated. These parameters were:1- the Elastic coefficient *E*, 2-viscoelastic coefficient η, and 3-geometry of the cross sections. These parameters were estimated from the literature that is primarily focused on experimental works [37, 38]. We integrated these parameters in the linear viscoelastic beam model, and good agreement was found with the experimental results of Alexandra et al [36]. We also integrated these parameters in the von Karman beam model for a filopodium crossing over an asperity. The distance sufficient to overcome the bending caused by the weight, when a filopodium is crossing an asperity was found. This study provided pertinent inputs for understanding filopodia protrusion and help better understanding of the interaction between living cells and prosthetic devices.

References

[1] C. R. Howlett, M. D. Evans, W. R. Walsh, G. Johnson and J. G. Steele, "Mechanism of initial attachment of cells derived from human bone to commonly used prosthetic materials during cell culture," *Biomaterials,* vol. 15, no. 3, pp. 213--222, 1994.

[2] H. Bernd, "Filopodia Focal Complexes Direct Adhesion and Force Generation Towards Filopodia Outgrowth," *Cell Adhesion & Migration,* vol. 4, no. 2, pp. 3839-3852, 2010.

[3] O. Medalia, M. Beck, M. Ecke, I. Weber, R. Neujahr, W. Baumeister and G. Gerisch, "Organization of actin networks in intact filopodia," *Current Biology,* vol. 17, no. 1, pp. 79-84, 2007.

[4] G. Gianluca, "Mechanisms Underlying the Initiation and Dynamics of Neuronal Filopodia: From Neurite Formation to Synaptogenesis," *International Review of Cell and Molecular Biology,* vol. 30, no. 1, pp. 95-156, 2013.

[5] C. Yang and T. Svitkina, "Filopodia initiation: focus on the Arp2/3 complex and formins," *Cell adhesion & migration,* vol. 5, no. 5, pp. 402-408, 2011.

[6] k. M. Pieta and P. Lappalainen, "Filopodia:Molecular architecture and cellular functions," *Nature Reviews Molecular Cell Biology,* vol. 9, no. 6, pp. 446-454, 2008.

[7] J. Albuschies and V. Vogel, "The role of filopodia in the recognition of nanotopographies," *Scientific Reports,* vol. 3, no. 1658, pp. 1-9, 2013.

[8] U. Schwarz, S. Safran and A. Samuel, "Physics of adherent cells," *Review of Modern Physics,* vol. 85, no. 3, pp. 1327-1381, 2013.

[9] I. Pavel, A. Zhuravlev and P. Garegin, "Protein fluxes along the filopodium as a framework for understanding the growth-retraction dynamics," *Cell Adhesion & Migration,* vol. 5, no. 5, pp. 448-456, 2011.

[10] A. Mogilner and B. Rubinstein, "The Physics of Filopodia Protrusion," *Biophysical Journal,* vol. 89, no. 2, pp. 782-795, 2005.

[11] W. William and M. Paul, "Structures in focus—filopodia," *The International Journal of Biochemistry & Cell Biology,* vol. 34, no. 7, pp. 726-730, 2002.

[12] S. Claudia, B. Bodo, B. Simone, M. Christoph, E. Eva-Maria and H. Bernd, "One step ahead: Role of filopodia in adhesion formation during cell migration of keratinocytes," *Experimental Cell Research,* vol. 315, no. 7, pp. 1212-1224, 2009.

[13] S. Yvonne, G. P. Solis and A. O. S. Claudia, "Regulation of focal adhesion formation and filopodia extension by the cellular prion protein (PrPC)," *FEBS Letters,* vol. 583, no. 2, pp. 389-393, 2009.

[14] C. A. Heckman and H. K. I. Plummer, "Filopodia as sensors," *Cellular Signalling,* vol. 25, no. 11, pp. 2298-2311, 2013.

[15] F. Jan, B. Dennis, T. E. B. Stradal and R. Klemens, "Filopodia: Complex models for simple rods," *The International Journal of Biochemistry & Cell Biology,* vol. 41, no. 8-9, pp. 1656-1664, 2009.

[16] T. Svitkina, "SpringerImages," Biology Image Library, 15 08 2008. [Online]. Available: http://www.springerimages.com/Images/Biomedicine/3-27475_0_Image16_BIL170608.

[17] R. W. Davenport, P. Dou, V. Rehder and S. Kater, "A sensory role for neuronal growth cone filopodia," *Nature Publishing Group,* 1993.

[18] H. Mellor, "The role of formins in filopodia formation," *Biochimica et Biophysica Acta,* vol. 1803, no. 2, pp. 191-200, 2010.

[19] D. Purves, G. J. Augustine and D. Fitzpatrick, The Axonal Growth Cone, Sunderland(MA): Sinauer Associates, 2001.

[20] M. Dalby, A. Hart, N. Gadegaad, C. Wilkinson and R. O. C. Oreffo, "Filopodial Sensing of Nanotopography in Osteoprogenitor Cells," *European Cells and Materials,* vol. 10, no. 2, p. 65, 2005.

[21] M. J. Dalby, M. O. Riehle, H. Johnstone, S. Affrossman and A. S. G. Curtis, "Investigating the limits of filopodial sensing: a brief report using SEM to image the interaction between 10 nm high nano-topography and fibroblast filopodia," *Cell Biology International,* vol. 28, pp. 229-236, 2004.

[22] J. Meyle, H. Wolburg and V. A. Recum, "Surface Micromorphology and Cellular Interactions," *Journal of Biomaterials Applications,* vol. 7, no. 4, pp. 362-374, 1993.

[23] A. Curtis and C. Wilkinson, "Topographical controls of cells," *Biomaterials,* vol. 18, no. 24, pp. 1573-1583, 1997.

[24] K. Anselme, P. Davidson, A. Popa, M. Giazzon, M. Liley and L. Ploux, "The interaction of cells and bacteria with surfaces structured at the nanometre scale," *Acta Biomaterialia*, vol. 6, no. 10, pp. 3824-3846, 2010.

[25] C. Chang-Hwan, H. H. Sepideh, M. W. Benjamin, D. C. Y. James, E. B. Ramin and C.-J. ". Ki, "Cell interaction with three-dimensional sharp-tip nanotopography," *Biomaterials*, vol. 28, no. 9, pp. 1672-1679, 2007.

[26] B. Thomas, R. Stephane, L. V. Christian, J. Jean-Francois, T. V. N. Guy and B. Patrica, "Filopodia retraction force generated by cortical actin dynamics and controlled by reversible tethering at the tip," *Proceedings of the National Academy of Sciences of United States of America*, vol. 110, no. 47, pp. 18928-18933, 2013.

[27] L. Yang, V. Chinthapenta, Q. Li, D. Stout, A. Liang, B. W. Sheldon and T. J. Webster, "Understanding osteoblast responses to stiff nanotopographies through experiment and computational simulations," *Journal of Biomedical Materials Research Part A*, vol. 97A, no. 4, pp. 375-382, 2011.

[28] Y. Lei, L. Qunyang, C. Viswanath, L. Amy, S. Brian W and J. W. Thomas, "The Impact of Material Nanotopography on Cell Functions and Filopodia Extension:," *Material Research Society*, vol. 1236, no. 10, p. 08, 2010.

[29] "Lecture note in Advanced variation in mechanics," University of Colorado at Boulder (Department of Aerospace Engineering Sciences).

[30] Y. Lan and G. A. Papoian, "The stochastic dynamics of filopodial growth," *Biophysical journal*, vol. 94, no. 10, pp. 3839-3852, 2008.

[31] R. Oldenbourg, K. Katoh and G. Danuser, "Mechanism of Lateral Movement of Filopodia and Radial Actin Bundles," *Biophysical Journal*, vol. 78, no. 3, pp. 1176-1182, 2000.

[32] H. M. Buettner, "Analysis of Cell-Target Encounter by Random," *Bioengineering,Food, and Natural Products*, vol. 42, no. 4, pp. 1127-1138, 1996.

[33] H. M. Buettner, "Computer Simulation of Nerve Growth Cone," *Cell Motility and the Cytoskeleton*, vol. 32, no. 3, pp. 187-204, 1995.

[34] P. H. Grimm, A. B. Verkhovsky, A. Mogilner and J. J. Meister, "Analysis of actin dynamics at the leading edge of crawling cells: implications for the shape of keratocyte lamellipodia," *European Biophysics Journal*, vol. 32, no. 6, pp. 563-577, 2003.

[35] N. Ozkaya, M. Nordin, D. Goldsheyder and D. Leger, Fundamentals of biomechanics: equilibrium, motion, and deformation, Springer Science & Business Media, 2012.

[36] A. Zidovska and E. Sackmann, "On the mechanical stabilization of filopodia," *Biophysical journal*, vol. 100, no. 6, pp. 1428-1437, 2011.

[37] X. Ying, C. L. Aih, D. M. Suter and U. L. Gil, "Topography and Nanomechanics of Live Neuronal Growth Cones Analyzed by Atomic Force Microscopy," *Biophysical Journal*, vol. 96, no. 12, pp. 5060-5072, 2009.

[38] A. J. Ridley, "Life at the Leading Edge," *Cell*, vol. 145, no. 7, pp. 1012-1022, 2011.

[39] B. Andreas and A. Ueli, "The structure of the F-actin filament and the actin molecule," *Current Opinion in Cell Biology*, vol. 4, no. 1, pp. 20-26, 1992.

[40] D. Roylance, "Engineering viscoelasticity," *Department of Materials Science and Engineering--Massachusetts Institute of Technology, Cambridge MA*, vol. 2139, pp. 1-37, 2001.

[41] I. Ana, G. A. Teixeira, J. D. McKie, P. J. Foley, P. F. Bertics, C. J. Nealey and Murphy, "The effect of environmental factors on the response of human corneal epithelial cells to nanoscale substrate topography," *Biomaterials*, vol. 27, no. 21, pp. 3945-3954, 2006.

[42] J. D. Matthew, G. Nikolaj, O. R. Mathis, D. W. Chris and S. C. Adam, "Investigating filopodia sensing using arrays of defined," *The International Journal of Biochemistry & Cell Biology*, vol. 36, no. 10, pp. 2005-2015, October 2004.

[43] P. Clark, P. Connolly, A. S. Curtis, J. A. Dow and C. D. Wilkinson, "Topographical control of cell behaviour: II. multiple grooved substrata," *Development*, vol. 108, no. 4, pp. 635-644, 1990.

[44] I. Ana, G. A. Teixeira, P. J. Abrams, C. J. Bertics, P. F. Murphy and Nealey, "Epithelial contact guidance on well-defined micro- and nanostructured substrates," *Journal of cell science*, vol. 116, no. 10, pp. 1881-1892, 2003.

Appendix A

A.1.4 By using the estimated Young's modulus and geometry of the cross section we obtain the values of axial and bending stiffness in tables below, for three values of the estimated diameter of the protrusion.

Table 6: Axial stiffness of a filopodium using the geometry and material parameters when the diameter is 100nm.

Young's modulus E kPa	Area A m^2	Axial stiffness EA N
20	$7.8593 \cdot 10^{-15}$	$1.5708 \cdot 10^{-10}$
30	$7.8593 \cdot 10^{-15}$	$2.3562 \cdot 10^{-10}$
40	$7.8593 \cdot 10^{-15}$	$3.1416 \cdot 10^{-10}$

Table 7: Axial stiffness of a filopodium using the geometry and material parameters when the diameter is 200nm.

Young's modulus E kPa	Area A m^2	Axial stiffness EA N
20	$3.1415 \cdot 10^{-14}$	$6.2383 \cdot 10^{-10}$
30	$3.1415 \cdot 10^{-14}$	$9.4248 \cdot 10^{-10}$
40	$3.1415 \cdot 10^{-14}$	$1.2566 \cdot 10^{-9}$

Table 8: Axial stiffness of a filopodium using the geometry and material parameters when the diameter is 300nm.

Young's modulus E Kpa	Area A m^2	Axial stiffness EA N
20	$7.0685 \cdot 10^{-14}$	$1.4173 \cdot 10^{-9}$
30	$7.0685 \cdot 10^{-14}$	$2.1206 \cdot 10^{-9}$
40	$7.0685 \cdot 10^{-14}$	$2.8274 \cdot 10^{-9}$

Different material and geometric parameters are reported in the tables below for the bending stiffness of the filopodium

Table 9: Bending stiffness of a filopodium using the geometry and material parameters when the diameter is 100nm.

Young's modulus E kPa	Area moment of inertia I m^4	Bending stiffness EI N
20	$4.908 \cdot 10^{-30}$	$9.817 \cdot 10^{-26}$
30	$4.908 \cdot 10^{-30}$	$1.4726 \cdot 10^{-25}$
40	$4.908 \cdot 10^{-30}$	$1.9685 \cdot 10^{-25}$

Table 10: Bending stiffness of a filopodium using the geometry and material parameters when the diameter is 200nm

Young's modulus E kPa	Area moment of inertia I m^4	Bending stiffness EI N
20	$7.8539 \cdot 10^{-29}$	$1.5708 \cdot 10^{-24}$
30	$7.8539 \cdot 10^{-29}$	$2.3562 \cdot 10^{-24}$
40	$7.8539 \cdot 10^{-29}$	$3.1416 \cdot 10^{-24}$

Table 11: Bending stiffness of a filopodium using the geometry and material parameters when the diameter is 300nm

Young's modulus E Kpa	Area moment of inertia I m^4	Bending stiffness EI N
20	$3.976 \cdot 10^{-28}$	$7.9523 \cdot 10^{-24}$
30	$3.976 \cdot 10^{-28}$	$1.1928 \cdot 10^{-23}$
40	$3.976 \cdot 10^{-28}$	$1.5904 \cdot 10^{-23}$